AGU PUBLICATIONS

JGR

Journal of Geophysical Research: Atmospheres

RESEARCH ARTICLE
10.1002/2015JD024567

**Key Points:**
- Upper tropospheric humidity alters the TOA flux diurnal cycle as strongly as vertical instability
- Clear-sky effects control TOA flux diurnal amplitude, while cloud forcing controls timing
- Disagreement in reanalysis monthly variability greatly affects assessment of TOA flux sensitivity

**Correspondence to:**
J. B. Dodson,
jason.b.dodson@nasa.gov

**Citation:**
Dodson, J. B., and P. C. Taylor (2016), Sensitivity of Amazonian TOA flux diurnal cycle composite monthly variability to choice of reanalysis, *J. Geophys. Res. Atmos.*, *121*, 4404–4428, doi:10.1002/2015JD024567.

Received 24 NOV 2015
Accepted 30 MAR 2016
Accepted article online 6 APR 2016
Published online 4 MAY 2016



# Sensitivity of Amazonian TOA flux diurnal cycle composite monthly variability to choice of reanalysis

**J. Brant Dodson[1] and Patrick C. Taylor[1]**

[1]NASA Langley Research Center, Hampton, Virginia, USA

**Abstract** Amazonian deep convection experiences a strong diurnal cycle driven by the cycle in surface sensible heat flux, which contributes to a significant diurnal cycle in the top of the atmosphere (TOA) radiative flux. Even when accounting for seasonal variability, the TOA flux diurnal cycle varies significantly on the monthly timescale. Previous work shows evidence supporting a connection between variability in the convective and radiative cycles, likely modulated by variability in monthly atmospheric state (e.g., convective instability). The hypothesized relationships are further investigated with regression analysis of the radiative diurnal cycle and atmospheric state using additional meteorological variables representing convective instability and upper tropospheric humidity. The results are recalculated with three different reanalyses to test the reliability of the results. The radiative diurnal cycle sensitivity to upper tropospheric humidity is about equal in magnitude to that of convective instability. In addition, the results are recalculated with the data subdivided into the wet and dry seasons. Overall, clear-sky radiative effects have a dominant role in radiative diurnal cycle variability during the dry season. Because of this, even in a convectively active region, the clear-sky radiative effects must be accounted for in order to fully explain the monthly variability in diurnal cycle. Finally, while there is general agreement between the different reanalysis-based results when examining the full data time domain (without regard to time of year), there are significant disagreements when the data are divided into wet and dry seasons. The questionable reliability of reanalysis data is a major limitation.

## 1. Introduction

Multiple processes contribute to the top of the atmosphere (TOA) diurnal cycle, and perhaps the most visibly obvious are clouds [*Gray and Jacobson*, 1977; *Janowiak et al.*, 1994; *Bergman and Salby*, 1996]. Clouds affect both shortwave and longwave radiation in a variety of ways depending on the cloud type, which influences the diurnal cycle timing [*Minnis and Harrison*, 1984; *Bergman and Salby*, 1997; *Loeb et al.*, 2009; *Taylor*, 2012]. One prominent example of the regionality in cloud diurnal cycle is the difference between convectively active tropical land and ocean [*Bergman and Salby*, 1996; *Yang and Slingo*, 2001; *Nesbitt and Zipser*, 2003; *Yang and Smith*, 2006]. Continental convective clouds often develop in the afternoon and evening and create extensive anvil clouds that persist through the night [*Tian et al.*, 2004; *Zhang et al.*, 2008]. In contrast, oceanic convection often (though not always) develops overnight and creates anvil regions that persist during the day. The effect of regionality in the cloud diurnal cycle on the shortwave budget is obvious; e.g., clouds occurring during night cannot affect the shortwave budget. The longwave effect can also be substantial; e.g., placing an optically thick high cloud over a warm daytime surface will have a larger longwave forcing effect than placing the same cloud over a cooler nighttime surface. Of course, the cloud effects coexist with clear-sky effects, such as the water vapor and surface temperature, which also have significant diurnal cycles.

There are two major reasons the TOA flux diurnal cycle must be understood—one observational and one modeling. The observational aspect involves the ability to precisely measure TOA fluxes using polar-orbiting, Sun-synchronous satellites [*Taylor and Loeb*, 2013]. These satellites cannot sample the full diurnal cycle, as each satellite sees each section of Earth twice per day (once for shortwave observations). The unobserved portions of the diurnal cycle must either be assumed or reconstructed from multiple polar-orbiting satellites combined with geostationary observations with high temporal resolution [e.g., *Doelling et al.*, 2013]. *Loeb et al.* [2009] indicate that error in the regional TOA fluxes can exceed 30 W $m^{-2}$ if the diurnal cycle is misrepresented. The second involves the ability to simulate the Earth system processes that give rise to the diurnal cycle. Many climate models, including general circulation models, have had significant difficulty in realistically simulating the convective diurnal cycle, particularly over land [e.g., *Chen et al.*, 1996; *Trenberth et al.*, 2003; *Sun et al.*, 2005; *Dai*, 2006; *Dirmeyer et al.*, 2012]. Errors exist in both phase and amplitude, and there is a frequent

"solar phase lock" error in which the precipitation diurnal cycle closely follows the insolation cycle instead of reproducing the observed ~3–6 h delay. In addition, propagating diurnal precipitation maxima, observed in the United States Great Plains [*Balling*, 1985] and Maritime Continent [*Yang and Slingo*, 2001; *Neale and Slingo*, 2003; *Itterly and Taylor*, 2014], generally do not occur in climate models. Understanding the processes that influence the TOA flux diurnal cycle will address the model shortcomings in simulating the convective diurnal cycle and their influence on climate.

The convective cloud diurnal cycle affects climate through its influence on the time-mean TOA energy budget and its variability. This includes monthly variability, which will be the focus of this paper. The impact of cloud diurnal cycles in the tropics on the time-mean outgoing longwave radiative (OLR) and reflected shortwave energy budget is estimated to be 1–5 and 5–15 W $m^{-2}$, respectively [*Bergman and Salby*, 1997; *Rozendaal et al*., 1995]. With respect to TOA flux variability, *Taylor* [2014a] found that variations in the diurnal cycle shape can contribute up to 7 W $m^{-2}$ or 10–80% of the regional monthly TOA flux standard deviation. The diurnal cycle contributions to TOA flux variability show significant regionality with convectively active land regions like the Amazon exhibiting the largest signal. The colocation of convective activity and large monthly variability suggests a causal connection between variability in radiative budget and variability in convective cloud properties.

One possible causal link involves the relationship between cloud properties and atmospheric state variables (ASVs). It has been well established in the literature, using both passive [*Raval et al*., 1994; *Bony et al*., 1997, 2004] and active radar [*Su et al*., 2008; *Del Genio et al*., 2012; *Dodson et al*., 2013] satellite observations, that variability in ASVs both drives and is driven by variability in clouds. *Taylor* [2014b] examined monthly changes in the observed TOA flux diurnal cycle as related to changes in monthly mean ASVs (using ERA-Interim for ASVs) and found that as much as 20% of variation in diurnal cycle shape (including amplitude and timing) arises from changes in atmospheric state influencing cloud type and coverage. For the Amazon region, *Taylor* [2014b] demonstrate that anomalously high (low) convective available potential energy (CAPE) tends to shift the outgoing longwave radiative (OLR) diurnal cycle earlier (later) in the day, and vice versa for lower tropospheric stability (LTS).

Major questions remain, however, about the robustness of these results. First, the reliance on reanalysis data raises a question about the reliability and potential influence of a reanalysis data set on the results. Would the conclusions hold when replicated using another reanalysis? There have been multiple studies that have shown significant disagreements between multiple reanalyses and reanalyses with observations [e.g., *Kennedy et al*., 2011; *Itterly and Taylor*, 2014; *Dolinar et al*., 2015; *Santanello et al*., 2015; *Jiang et al*., 2015]. Second, there may be other ASVs, not tested by *Taylor* [2014b], that influence the monthly variability of the TOA radiative diurnal cycle as strongly as CAPE and LTS. Because deep convection connects the lower and upper troposphere, it is possible that upper tropospheric ASVs may have a significant influence on the convective cloud diurnal cycle. Upper level ASVs would be involved primarily in influencing and being influenced by the properties of convective anvils after formation from convective towers. Because convective anvils can persist for hours after deep convection ceases, monthly variability in their evolution may have significant effects on the radiative diurnal cycle. In addition, it is possible that upper level large-scale advection of ASVs may contribute to monthly variability in convective cloud properties [e.g., *Mapes and Zuidema*, 1996] and therefore radiative diurnal cycle variability. Because of these factors, we have chosen to expand the investigation by *Taylor* [2014b] to include both other reanalysis data sets and additional ASVs that represent the state of the upper troposphere.

For this study, we have selected Amazonian South America as the convective continental region. This region is of particular interest because of the large contribution of the TOA flux diurnal cycle to the mean TOA flux, but there are other useful properties as well. The Amazon has frequent deep convection during austral summer, with a prominent dry season during winter [*Yang and Slingo*, 2001]. The frequent summertime convection provides a large number of opportunities for satellite observations, from which to calculate reliable statistics. Furthermore, Amazonian convection has a relatively uniform diurnal cycle of convection across most of the region, with only small regions of nocturnal precipitation maxima in the northeast corner and western mountains. There is little evidence of an inhomogeneous propagating or terrain-induced diurnal peaks across the much of the Amazon, like those found in central North America, southeast China, or the Maritime Continent [*Yang and Smith*, 2006; *Dirmeyer et al*., 2012; *Itterly and Taylor*, 2014]. Thus, any investigation of the Amazonian diurnal cycle of convection will not be strongly influenced by such irregularities, nor will any

modeling study of the region be required to account for them. In addition, the wet/dry season contrast allows for a comparison of the statistical results in regional atmospheres with significantly different properties, to test the idea that the convective diurnal cycle is the primary control on the TOA flux diurnal cycle—if this is true, then the relationships between the TOA flux diurnal cycle and ASV variability should be larger in the wet than dry season.

It should be noted that the results and conclusions presented in this paper apply for the Amazon and may not necessarily represent the other regions of Earth. This includes other convectively active tropical continental regions, such as tropical Africa. While examination of other global regions is a worthy topic of research, it is beyond the scope of this paper.

This paper describes the effort to test and expand upon the results found by *Taylor* [2014b] and thus further test the hypothesis that monthly variability in the radiative diurnal cycle is largely a result of relationships between clouds, ASVs, and radiation. In particular, we will answer three main questions. First, are the results from *Taylor* [2014b] robust when replicated using other reanalysis data sets? Second, are there other ASVs that influence the monthly variability of the diurnal cycle as strongly as the ones examined by *Taylor* [2014b], including upper tropospheric ASVs? And finally, what is the seasonal dependence of these results?

We have organized our investigation and results as follows. Section 2 describes the data sets, which include Clouds and Earth's Radiant Energy System (CERES) data augmented with geostationary satellite data and three reanalysis data sets. Section 3 describes the methodology; while it is adapted from that of *Taylor* [2014b], there are some minor but important differences. Section 4 expands upon the previous work in two main ways. We will examine the difference of results from using different reanalysis products and also examine additional ASVs. These ASVs include upper tropospheric humidity, representing the upper troposphere's effect on radiative variability, and alternative measures of vertical stability, which is a difficult atmospheric property to reliably estimate from reanalysis data. Section 5 will present the seasonal variability of the results shown in section 4. Section 6 includes discussion on various topics related to the results, including potentially identifying the underlying causes. Our conclusions are presented in section 7.

## 2. Data

### 2.1. CERES SYN1deg

The TOA radiative flux data used in this study are taken from the CERES SYN1deg set of products [*Doelling et al.*, 2013]. This data set combines observations from CERES, the Moderate Resolution Imaging Spectroradiometer (MODIS), and geostationary imaging satellites to produce global gridded maps of several TOA radiative variables (RVs) [*Loeb et al.*, 2009]. The horizontal resolution is $1° \times 1°$, and the temporal resolution is 3-hourly.

Monthly mean data are supplied by CERES SYN1deg-Month Ed3A, and the monthly mean diurnal cycle data (at 3 hour intervals) are taken from CERES SYN1deg-M3Hour Ed3A. The RVs used are total-sky OLR, clear-sky OLR (OLRC), total-sky reflected shortwave (RSW), clear-sky reflected shortwave (RSWC), longwave cloud forcing (LWCF), and shortwave cloud forcing (SWCF). The latter two are calculated as OLRC-OLR and RSWC-RSW, respectively. From the shortwave variables we calculate total-sky albedo ($\alpha$), clear-sky albedo ($\alpha$C), and cloud albedo ($\alpha$L), which are obtained by normalizing RSW, RSWC, and SWCF (respectively) by solar irradiance.

According to *Doelling et al.* [2013], the monthly RMS errors for the shortwave and longwave TOA fluxes with respect to Geostationary Earth Radiation Budget (GERB) measurements [*Harries et al.*, 2005] are 3.5 and 0.53 W m$^{-2}$, respectively (their Table 4). Note that 3.5 W m−2 corresponds with ~1.0% albedo. While the 3 h instantaneous measurement RMS errors are larger than the monthly errors, keep in mind that we are averaging data to produce monthly diurnal cycle anomalies, so the monthly RMS errors are more relevant than the 3 h errors. Furthermore, the main sources of the monthly RMS error are from features such as the Sahara Desert and are not associated with tropical convection. Older versions of the CERES data sets, which lacked geostationary calibration, were more susceptible to the influence of tropical convection, contributing to biases greater than 5 W m$^{-2}$ during the (convectively active) afternoon in tropical Africa [*Doelling et al.*, 2013, Figure 8]. But the shift to geostationary calibration has reduced the error to 1 W m$^{-2}$ at all times of day. Errors in CERES observation of the diurnal cycle (relative to GERB) are at least an order of magnitude smaller than the amplitude of the diurnal cycle.

### 2.2. Reanalysis Data

The Modern-Era Retrospective Analysis for Research and Applications (MERRA) reanalysis product [*Rienecker et al.*, 2011] was designed to better simulate the global hydrological cycle than previously existing reanalyses and places a specific focus on assimilating modern NASA Low Earth Orbit satellite data. The horizontal resolution for the products we use is 0.67° in longitude by 0.5° in latitude, and vertical profiles are represented with a 42-level pressure grid with variable spacing and 3-hourly time resolution. While precipitation and surface fluxes are still problematic, as they are unconstrained, other aspects of the hydrological cycle have been improved to more closely resemble raw observations. Work using the Microwave Limb Sounder found a 10% moist bias in mixing ratio for MERRA over the Amazon at 215 hPa [*Jiang et al.*, 2015].

Detrending the MERRA data is necessary. Several ASVs in MERRA have clear trends in the Amazon region which are both statistically and physically significant but may be spurious and do not appear in the other reanalysis data. We describe the details of this in Appendix A.

The Interim European Center for Medium Range Weather Forecasts Re-Analysis (ERA-I) [*Dee et al.*, 2011] provides global data from 1978, at 0.75° × 0.75° horizontal resolution, 60 pressure levels, and 3-hourly time resolution. ERA-I uses the IFS model, a T255 spectral model. CAPE is provided as an output variable. The data are detrended as with MERRA; however, the data do not show any significant decadal trends.

The National Center for Environmental Prediction/National Center for Atmospheric Research Reanalysis (NNR) [*Kalnay et al.*, 1996] provides global reanalysis data from 1948 to present at a 2.5° × 2.5° horizontal resolution, at 17 pressure levels, and with 6 h time resolution. The model used is a T62 global spectral model, and data are assimilated from multiple satellites and in situ sources. As with MERRA, CAPE is not provided by NNR and must be computed separately. As with ERA-I, the data are detrended even though there are no significant trends in any data field.

## 3. Methodology

The methodology we use is adapted from *Taylor* [2014b], where the relationships between RVs and ASVs are expressed as linear regression slopes of the monthly mean values. Before the regressions are calculated, we first calculate the mean seasonal cycle of ASVs and RVs and remove it from the raw data; the resulting quantities are monthly departures from the seasonal cycle, represented as [var]′. Also, the time and space domains for the Amazon region remain unchanged. The spatial domain is (0.0°–25.0°S, 50.0°–70.0°W), and the time period under consideration is July 2002 to October 2012.

The relationship between the TOA flux diurnal cycle and lower tropospheric atmospheric state is investigated using several ASVs. Two ASVs used by *Taylor* [2014b] are also used here—namely, CAPE (a vertically integrated measure of convective instability related to the temperature difference between a pseudoadiabatically lifted parcel and environment) and LTS (LTS = $\theta_{700} - \theta_{sfc}$, where $\theta$ is potential temperature). For all reanalyses, CAPE is calculated using the most unstable boundary layer parcel. In addition, we include a deep tropospheric analog to LTS, free tropospheric stability (FTS), defined as FTS = $\theta_{E250} - \theta_{E850}$, where $\theta_E$ is the equivalent potential temperature. Because CAPE is a vertically integrated quantity, small errors in temperature and humidity can lead to large errors in CAPE when the absolute magnitude is small [*Doswell and Rasmussen*, 1994]. This has important consequences for reanalysis output, which have inconsistent observational constraints on various atmospheric and surface quantities rendering reanalysis estimates of CAPE unfortunately unreliable. Because FTS is intended to represent deep layer vertical stability, we expect that FTS-based results will closely resemble CAPE-based results.

These ASVs represent lower tropospheric forcing/inhibition of deep convective cores (DCCs). However, once deep convection terminates, or once the anvil cloud is transported far from the convection, lower tropospheric ASVs cease to directly influence the remnant anvil cloud properties, and upper tropospheric ASVs may become an important influence.

We have tested multiple ASVs that characterize the upper troposphere to investigate the potential influence on the TOA flux diurnal cycle. The ASV with the greatest reliably identifiable influence is upper tropospheric relative humidity (UTH) which is a common ASV in studies of high-level clouds, including convective anvils [e.g., *Soden and Fu*, 1995; *Zhu et al.*, 2000; *Sassi et al.*, 2001; *Tian et al.*, 2004]. Increased UTH can influence clouds

**Table 1.** Regression Slopes of RVLW′/ASV′[a]

| | | OLR′ | | | OLRC′ | | | LWCF′ | | |
|---|---|---|---|---|---|---|---|---|---|---|
| RVLW′ (W/m$^2$) | | Quad | Wet | Dry | Quad | Wet | JJA | Quad | Wet | Dry |
| /CAPE′ | MERRA | −0.56 | −0.04 | ***−3.14*** | −0.24 | −0.30 | **−0.90** | *0.45* | 0.06 | ***2.24*** |
| | ERA-I | ***−1.79*** | *−1.55* | ***−3.12*** | ***−0.63*** | −0.53 | **−1.07** | ***1.28*** | **1.27** | ***2.05*** |
| | NNR | −0.52 | 0.09 | −1.22 | −0.14 | −0.15 | −0.24 | *0.51* | 0.12 | 0.97 |
| /FTS′ | MERRA | ***1.11*** | −0.59 | **2.33** | ***0.46*** | 0.17 | **1.07** | **−0.68** | 0.48 | **−1.25** |
| | ERA-I | ***1.80*** | ***2.28*** | ***2.93*** | ***0.60*** | ***1.03*** | **0.99** | ***−1.25*** | ***−1.47*** | ***−1.94*** |
| | NNR | **1.46** | **1.83** | **2.19** | **0.42** | *0.62* | *0.76* | ***−1.01*** | **−1.06** | **−1.43** |
| /LTS′ | MERRA | −0.08 | 0.09 | −0.87 | −0.24 | −0.27 | −0.52 | −0.10 | −0.21 | 0.34 |
| | ERA-I | ***−1.68*** | −1.24 | *−2.29* | ***−0.85*** | ***−0.90*** | ***−1.19*** | ***0.87*** | 0.54 | *1.11* |
| | NNR | −0.14 | *1.51* | *−1.63* | −0.26 | 0.37 | **−1.01** | −0.08 | *−0.99* | 0.62 |
| /RH250′ | MERRA | ***−2.72*** | ***−2.30*** | ***−4.03*** | ***−1.21*** | ***−1.17*** | ***−1.89*** | ***1.58*** | ***1.39*** | ***2.13*** |
| | ERA-I | ***−3.39*** | ***−3.38*** | ***−4.21*** | ***−1.37*** | ***−1.01*** | ***−2.17*** | ***1.93*** | ***2.06*** | ***2.04*** |
| | NNR | ***−3.07*** | ***−2.92*** | ***−4.35*** | ***−1.32*** | ***−0.87*** | ***−2.06*** | ***1.69*** | ***1.72*** | ***2.29*** |

[a]Results for the quadra-season (QUAD), wet season (WET), and dry season (DRY). ASVs are normalized by standard deviation. Statistically significant values are noted as follows: $0.05 > p \geq 0.10$ are italicized, $0.01 > p \geq 0.05$ are bolded, and $p \geq 0.01$ are bolded and italicized.

by decreasing the evaporation rate of ice crystals, prolonging cloud lifetime. Conversely, the increased presence of both high clouds and DCCs can increase UTH through increased evaporation and direct humidity transport.

We represent UTH with the 250 hPa relative humidity (RH250). While 250 hPa is below the level of maximum convective detrainment [*Folkins and Martin*, 2005; *Fueglistaler et al*., 2009], it is still well within the outflow layer. Sensitivity tests using relative humidity data from different altitudes (not shown) reveal that the results are mostly independent of altitude below 150 hPa. The 150 hPa level is above the altitude of maximum detrainment, and it is of sufficient altitude for the physics of the tropical tropopause layer to influence the variability of relative humidity.

To determine the influence of ASVs on the diurnal cycle of RVs, we regress the CERES SYN1deg diurnal cycle of the RVs against the reanalysis ASVs (indicated as $[RV]_{DC}'/[ASV]'$). We subtract the mean regression slope values from the diurnal cycle of regression slopes (Tables 1 and 2) to highlight the sensitivity of the RV′ diurnal cycles to variability in ASV′. No attempt is made to smooth the diurnal cycle data or approximate the cycles with harmonics. In addition, we represent variability in the ASVs as standard deviations rather than raw values. This yields a more intuitive view of which regression slopes have a larger effect on the RV′ diurnal cycle. The values for the standard deviations are shown in Table 3.

Figure 1 shows the mean diurnal cycles of the RVs in the Amazon for the total year (i.e., the quadra-season, including wet, dry, and transition seasons), the December-January-February season (the wet season), and the June-July-August season (the dry season). For this paper, we denote the diurnal cycle of all variables

**Table 2.** Regression Slopes of RVSW′/ASV′[a]

| | | $\alpha'$ | | | $\alpha C'$ | | | $\alpha L'$ | | |
|---|---|---|---|---|---|---|---|---|---|---|
| RVSW′ (%) | | Quad | Wet | Dry | Quad | Wet | JJA | Quad | Wet | Dry |
| /CAPE′ | MERRA | 0.00 | 0.05 | *0.32* | ***−0.05*** | ***−0.06*** | −0.06 | 0.05 | 0.12 | *0.37* |
| | ERA-I | 0.07 | −0.15 | *0.32* | −0.02 | 0.02 | −0.05 | 0.10 | −0.17 | **0.38** |
| | NNR | −0.12 | −0.24 | 0.01 | −0.02 | 0.00 | *−0.08* | −0.10 | −0.24 | 0.09 |
| /FTS′ | MERRA | −0.08 | 0.03 | −0.26 | ***−0.08*** | 0.04 | ***0.19*** | *−0.15* | 0.00 | **−0.46** |
| | ERA-I | −0.12 | *−0.30* | −0.22 | **0.05** | 0.00 | **0.11** | *−0.18* | −0.29 | *−0.33* |
| | NNR | −0.12 | ***−0.50*** | −0.15 | 0.00 | 0.00 | *0.08* | −0.13 | ***−0.50*** | −0.22 |
| /LTS′ | MERRA | *0.18* | 0.20 | *0.30* | −0.04 | ***−0.07*** | 0.00 | 0.22 | 0.27 | 0.30 |
| | ERA-I | ***0.48*** | *0.32* | ***0.53*** | **−0.04** | ***−0.06*** | 0.02 | ***0.52*** | **0.38** | ***0.51*** |
| | NNR | **0.21** | −0.28 | ***0.50*** | **−0.05** | **−0.05** | 0.00 | ***0.25*** | −0.23 | ***0.49*** |
| /RH250′ | MERRA | ***0.35*** | **0.39** | ***0.57*** | **−0.05** | **−0.05** | *−0.08* | ***0.39*** | **0.43** | ***0.65*** |
| | ERA-I | ***0.50*** | ***0.51*** | ***0.65*** | *−0.03* | 0.00 | *−0.08* | ***0.54*** | ***0.51*** | ***0.73*** |
| | NNR | ***0.47*** | ***0.46*** | ***0.57*** | ***−0.06*** | 0.00 | ***−0.12*** | ***0.53*** | **0.45** | ***0.69*** |

[a]As in Table 1 but for shortwave RVs.

**Table 3.** Total Standard Deviation of ASVs

| STDDEV | | Quad | Wet | Dry |
|---|---|---|---|---|
| CAPE′ (J kg$^{-1}$) | MERRA | 88.34 | 91.47 | 89.28 |
| | ERA-I | 65.79 | 54.35 | 77.38 |
| | NNR | 40.87 | 32.98 | 46.17 |
| FTS′ (K) | MERRA | 0.94 | 0.50 | 1.27 |
| | ERA-I | 0.88 | 0.52 | 1.14 |
| | NNR | 0.81 | 0.65 | 0.93 |
| LTS′ (K) | MERRA | 0.60 | 0.67 | 0.59 |
| | ERA-I | 0.38 | 0.26 | 0.46 |
| | NNR | 0.37 | 0.21 | 0.49 |
| RH250′ | MERRA | 0.025 | 0.021 | 0.031 |
| | ERA-I | 0.031 | 0.024 | 0.040 |
| | NNR | 0.027 | 0.023 | 0.037 |

as $[\mathrm{var}]_{DC}$. The quadra-season results correspond to Figures 1c and 1d from *Taylor* [2014b]. The amplitude of $LWCF_{DC}$ (calculated as maximum minus minimum values) is larger than $OLRC_{DC}$, though not greatly, so both contribute to $OLR_{DC}$. As with other tropical continental regions, $OLRC_{DC}$ follows the diurnal cycle of surface radiation from solar heating, which is much larger for land than ocean. However, unlike non-convective tropical continental regions, afternoon convection creates a large

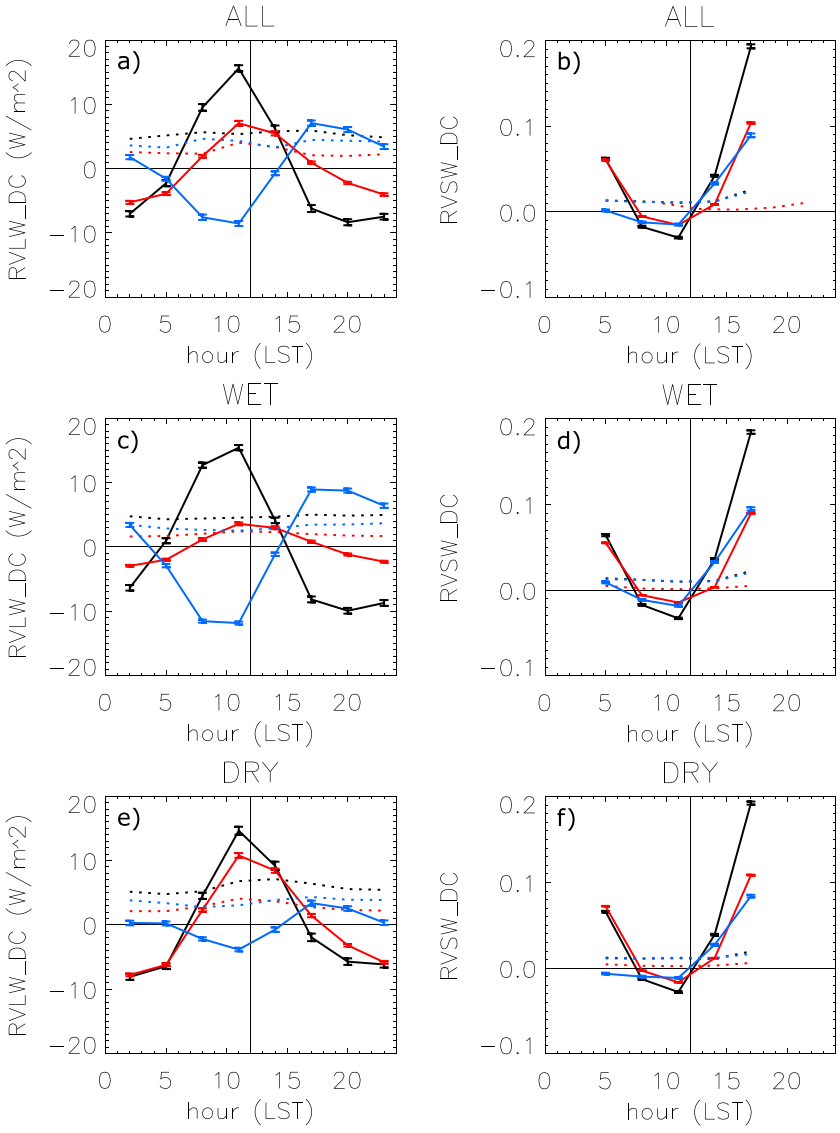


**Figure 1.** The deseasonalized 3-hourly diurnal cycles of (a, c, and e) longwave and (b, d, and f) shortwave TOA radiation for the quadra-season (Figures 1a and 1b), the wet season (December-January-February, DJF, Figures 1c and 1d), and the dry season (June-July-August, JJA, Figures 1e and 1f), as derived from CERES SYN-1deg. On left, $OLR_{DC}$′ is shown in black, $OLRC_{DC}$′ in red, and $LWCF_{DC}$′ in blue. On the right, $\alpha_{DC}$′ is shown in black, $\alpha C_{DC}$′ in red, and $\alpha L_{DC}$′ in blue. Solid (dotted) lines are the mean (standard deviation). Error bars represent the 1$\sigma$ standard error.

$LWCF_{DC}$ that offsets $OLR_{DC}$ earlier in the day than it would be from clear-sky radiation alone. During the wet (dry) season, $LWCF_{DC}$ grows (shrinks) in amplitude and $OLRC_{DC}$ shrinks (grows), meaning that $LWCF_{DC}$ has an increased (decreased) dominance in shaping $OLR_{DC}$. This is reasonable when considering the much greater frequency of convection during the wet than dry season.

To assess the aforementioned differences in the reanalyses, Figure 2 shows the PDFs of the ASV anomalies during the quadra-season, wet, and dry seasons and lists the mean values and standard deviations. Note that all data are accounted for in the plots, even if some of the plots appear truncated. One interesting feature of the mean values is that MERRA shows the largest convective instability if CAPE is used as a metric, but ERA-I has the greatest instability if FTS is used. As demonstrated elsewhere in this paper, it raises the question of how useful CAPE is as a metric for convective activity, at least when calculated from reanalysis output. The results also demonstrate the biases in RH250, which were discussed previously. UTH in tropical continental regions is closely connected with convective activity [*Sassi et al.*, 2001], and the disagreement in mean UTH between the reanalyses is almost certainly connected with the differing treatments of convection. However, the differences in data assimilation sources cannot be ruled out either, and determining the cause of the disagreements is beyond the scope of this paper. It should be noted that the mean values are removed from the data used in this paper, so these biases do not directly affect the results and conclusions presented here.

The quadra-season results show normal distributions with similar standard deviations between the reanalyses for most ASVs. MERRA has slightly more spread than NNR and ERA-I for CAPE and noticeably more for LTS. The PDFs for the wet and dry seasons do not fit the normal distribution as closely, likely because of the limited number of months (~30) when compared with the quadra-season time domain (124). But the standard deviations are still for the most part similar between the reanalyses for the different ASVs. The most obvious exception is LTS during the wet season, where the standard deviation for MERRA (1.2 K) is 6 times that of NNR (0.2 K). In addition, MERRA produces a standard deviation for CAPE during the wet season (169 J $kg^{-1}$) that is 3 times that of NNR (53 J $kg^{-1}$). For other ASVs during the wet season, and all ASVs during the dry season, the disagreement in standard deviation between reanalyses is within 100%. Overall, it appears that when the mean and seasonal biases are removed, all three reanalyses produce similar ranges of monthly variability (i.e., similar climates), with the exception of LTS during the wet season.

As noted previously, MERRA and ERA-I data are provided at 3-hourly time resolution, while NNR is provided at 6-hourly. We tested for the possibility that the differing time resolutions may be a source of disagreement for NNR versus ERA-I and MERR by reducing the resolution of the latter two to 6-hourly. The statistics of 6-hourly versus 3-hourly resolutions for both ERA-I and MERRA change by less than 1%. Thus, we can be reasonably sure that the difference in time resolution does not cause spurious disagreements between reanalyses.

## 4. Results From Expanded Analysis of ASVs

First, we attempt to replicate the results of *Taylor* [2014b] using MERRA and NNR data. This includes the use of FTS and RH250 to represent convective instability and upper tropospheric conditions, respectively.

### 4.1. CAPE

Figure 3 displays the diurnal variability for all seasons in $RV_{DC}$′/CAPE′, which indicates the change in sensitivity of the TOA flux to monthly variability in convective instability over the course of the day. Notice that $OLR_{DC}$′/CAPE′, $OLRC_{DC}$′/CAPE′, and $LWCF_{DC}$′/CAPE′ have sine-like curves, similar to the mean diurnal cycles of OLR′, OLRC′, and LWCF′. When the diurnal timing of the maxima and minima of $RVLW_{DC}$′/ASV′ and $RVLW_{DC}$′ coincides (opposes), then positive ASV′ amplifies (reduces) $RVLW_{DC}$′. For example, the ERA-I results show that positive CAPE′ amplifies $LWCF_{DC}$′ and reduces $OLRC_{DC}$′. When the diurnal timing of the maxima and minima of $RVLW_{DC}$′/ASV′ and $RVLW_{DC}$′ misaligns by several hours, then positive ASV′ shifts $RV_{DC}$′ earlier and later in the day. The ERA-I results show that positive CAPE′ shifts $OLR_{DC}$′ earlier in the day (on the order of an hour). In other words, months with anomalously high convective instability will have a larger diurnal cycle in cloud radiative forcing, and a smaller diurnal cycle in clear-sky radiative cooling, leading to an earlier peak in OLR′. These diurnal stretch/shrink/shift relationships also appear when using a percentile-based methodology (not shown), so they are not simply an artifact of the regression analysis.

$RVSW_{DC}$′/ASV′ can be interpreted in a similar manner. However, because $RVSW_{DC}$′ occurs over only half a day and is strongly dependent on solar angle, it is better to conceptualize the interaction of $RVSW_{DC}$′/ASV′ and

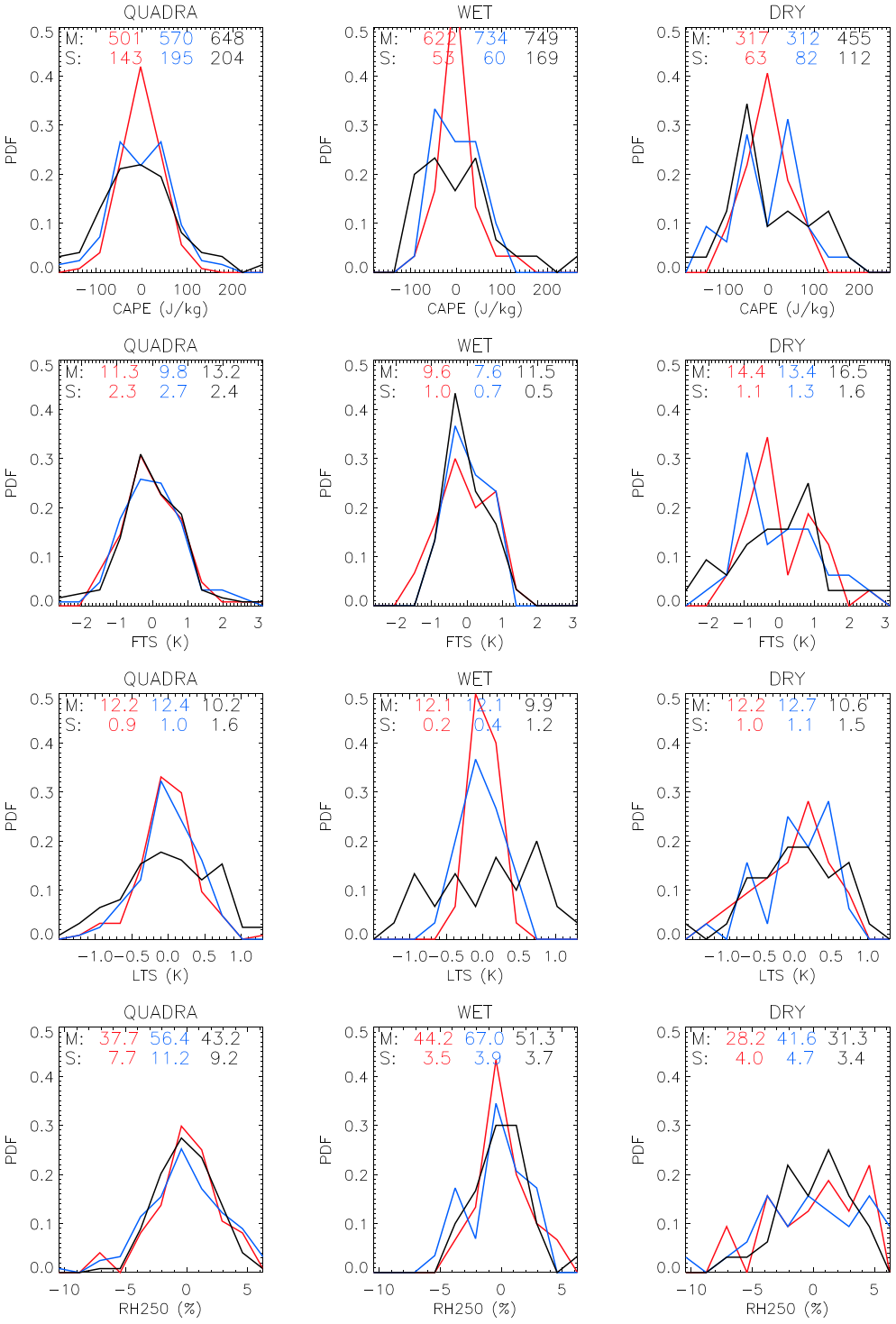


**Figure 2.** PDFs of (first row) CAPE′, (second row) FTS′, (third row) LTS′, and (fourth row) RH250′, for the (left column) quadra-season, (middle column) wet season, and (right column) dry season. NNR is shown in red, ERA-I in blue, and MERRA in black. The long-term mean values (*M*) and standard deviations (*S*) are shown for each ASV and season.

$RVSW_{DC}$′ as shifting the preference of high $\alpha$′ between morning, noon, and afternoon. For example, ERA-I shows that positive CAPE′ increases (decreases) $\alpha$′ in the afternoon (morning). Note that this does not necessarily imply that the monthly mean albedo anomaly itself is positive (negative) in the afternoon (morning) but just that the albedo diurnal cycle shape is changing.

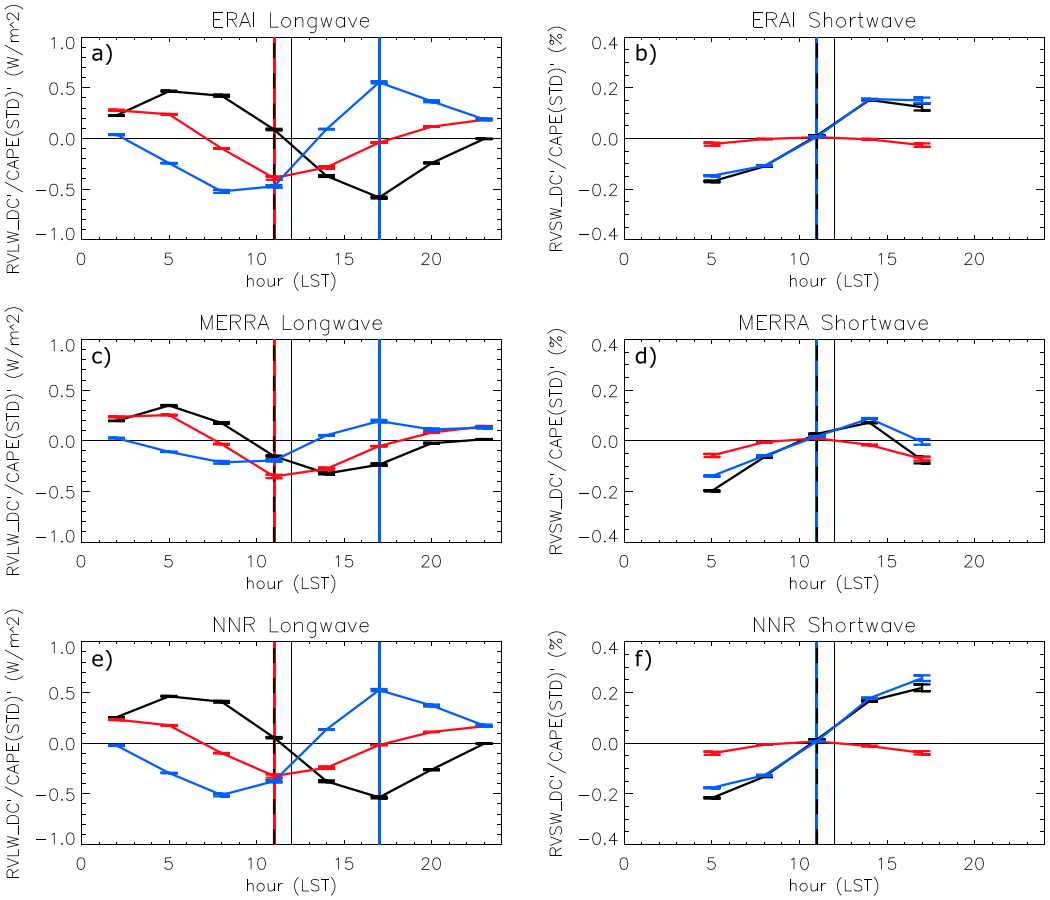


**Figure 3.** The 3-hourly diurnal variability in the $RV_{DC}$'/CAPE' regression slopes, for the quadra-season (no seasonal subsetting). On the left, $OLR_{DC}$'/CAPE' is shown in black, $OLRC_{DC}$'/CAPE' in red, and $LWCF_{DC}$'/CAPE' in blue. On the right, $\alpha_{DC}$'/CAPE' is shown in black, $\alpha C_{DC}$'/CAPE' in red, and $\alpha L_{DC}$'/CAPE' in blue. CAPE is taken from (a, b) ERA-I, (c, d) MERRA, and (e, f) NNR. All slope values are normalized by the standard deviation of the ASVs (as shown in Table 3). Vertical lines represent the diurnal time of maximum (minimum) for $OLR_{DC}$', $OLRC_{DC}$', and $LWCF_{DC}$' ($\alpha_{DC}$', $\alpha C_{DC}$', and $\alpha L_{DC}$').

The diurnal variations of the $RVLW_{DC}$'/CAPE' relationships share multiple similarities between the three reanalyses. The greatest similarity exists in $OLRC_{DC}$'/CAPE', which is almost identical between the three. $OLRC_{DC}$'/CAPE' is negative in the afternoon and positive in the evening and early morning. This behavior may be due to either increased water vapor in the clear-sky areas from nearby deep convection or a cooler surface in the afternoon from deep convective outflow.

There is less agreement on the values of $LWCF_{DC}$'/CAPE'. All three reanalyses show the same phase, but MERRA has less than half the amplitude of ERA-I and NNR. $LWCF_{DC}$'/CAPE' bottoms around the same time for all three reanalyses, but MERRA peaks about 3 h later (2300 local standard time (LST) versus 2000 LST). Both reanalyses show a negative $LWCF_{DC}$'/CAPE' occurring from morning to noon. The increased sensitivity of $LWCF_{DC}$'/CAPE' in the afternoon/evening is consistent with the role of increased CAPE causing increased deep convective activity.

The LWCF' and OLRC' effects combined lead to an $OLR_{DC}$'/CAPE' minimum (more negative) in the afternoon/evening and a maximum in midmorning. The maximum/minimum times in $OLR_{DC}$'/CAPE' do not match with the maximum/minimum time in $OLR_{DC}$', meaning that increased CAPE' tends to shift the $OLR_{DC}$' maximum/minimum times earlier in the day than average. The smaller amplitude of $LWCF_{DC}$'/CAPE' in MERRA results in a smaller $OLR_{DC}$'/CAPE' amplitude and thus a smaller shifting of $OLR_{DC}$' with increased CAPE'.

As with $RVLW_{DC}$'/CAPE', $RVSW_{DC}$'/CAPE' shows broadly similar results between the reanalyses, with MERRA being slightly different from the others. The $\alpha_{DC}$'/CAPE' and $\alpha L_{DC}$'/CAPE' daytime cycles follow each other closely through most of the day, transitioning from negative at morning to positive in the afternoon. As with

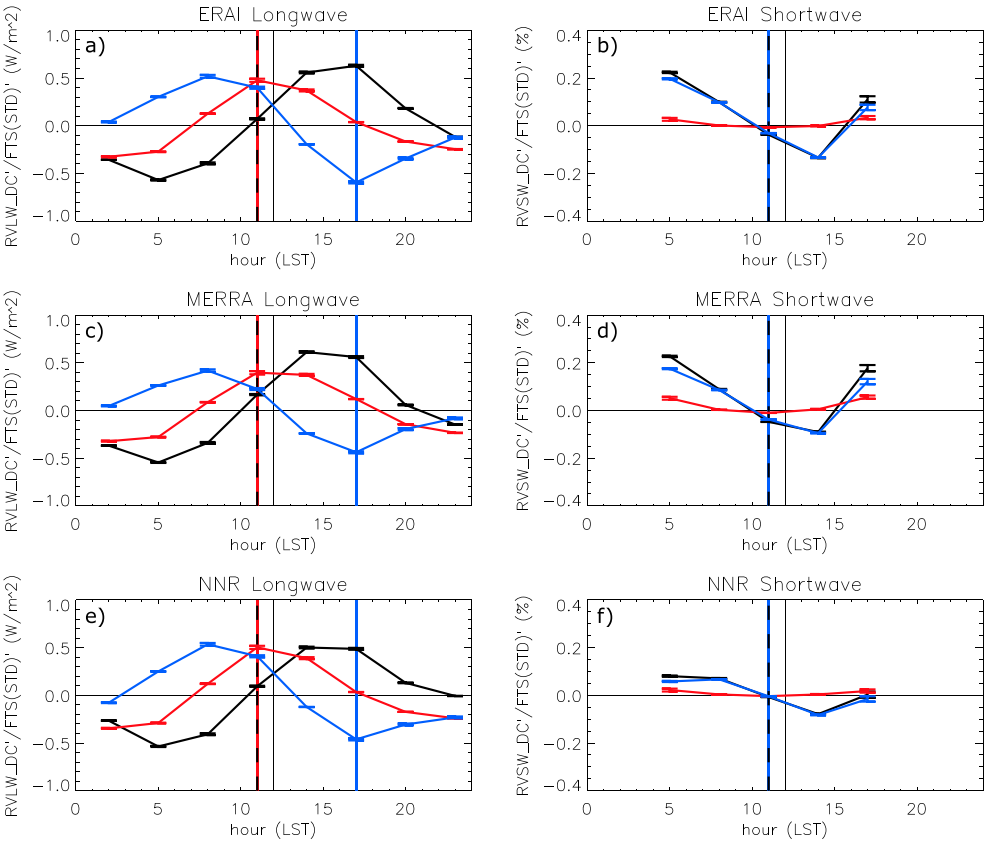


**Figure 4.** As in Figure 3 but with FTS′ as the ASV.

$LWCF_{DC}$′/CAPE′, this is probably the effect of increased sensitivity in the afternoon from convective activity, which causes a larger difference between the morning and afternoon $\alpha_{DC}$′ and $\alpha L_{DC}$′ values when CAPE′ > 0. The $\alpha C_{DC}$′/CAPE′ cycle is notably smaller than the other two, indicating that clouds are almost exclusively the controlling factor for $\alpha_{DC}$′. The main disagreement in reanalyses occurs in the later afternoon. MERRA shows a decrease in $\alpha L_{DC}$′/CAPE′ from 1400 to 1700 LST, while NNR shows an increase, and ERA-I shows little change.

The TOA insolation at 1700 LST is about a quarter of that at noon, so a significant discrepancy at this time may be important. Unfortunately, it is not apparent from these results what may be the cause. This time of day is past the time of maximum precipitation and is when the vigorous DCCs of early afternoon are either dissipating or transforming into mesoscale convective systems (MCSs). One obvious explanation for the disagreement in $\alpha L_{DC}$′/CAPE′ between the reanalysis at 1700 LST is that the DCC-to-MCS transition period is highly sensitive to CAPE′, and the discrepancies in CAPE′ between the reanalyses result in the disagreement in $\alpha L_{DC}$′/CAPE′. The discrepancy in $\alpha L_{DC}$′/CAPE′ is larger than $LWCF_{DC}$′/CAPE′ because anvil clouds, which coexist with and overlap the MCSs, obscure the longwave emission of the MCSs more strongly than the reflected shortwave. If this is true, then the methodology does not clearly capture the relationship between $\alpha$ and the DCC-to-MCS portion of the convective cycle.

### 4.2. FTS

Small errors in the temperature and humidity profile can lead to large errors in CAPE, which can render the reanalysis-based CAPE unreliable. Therefore, a new measure of deep tropospheric vertical instability, FTS, was created as an alternative. If FTS and CAPE represent the same physical atmospheric property, then we expect the $RV_{DC}$′/FTS′ results to resemble $RV_{DC}$′/CAPE′ results (this idea is tested in section 6). The curves would be mirror images, reflected across the *x* axis, because positive FTS′ indicates increased stability while increased CAPE′ indicates decreased stability. This is generally what we see in the $RVLW_{DC}$′-based results (Figure 4). For ERA-I and NNR, the $RVLW_{DC}$′/FTS′ curves are almost the mirror image of the $RVLW_{DC}$′/CAPE′ curves, sharing the same amplitudes and phases. The situation is more complicated with MERRA. While the

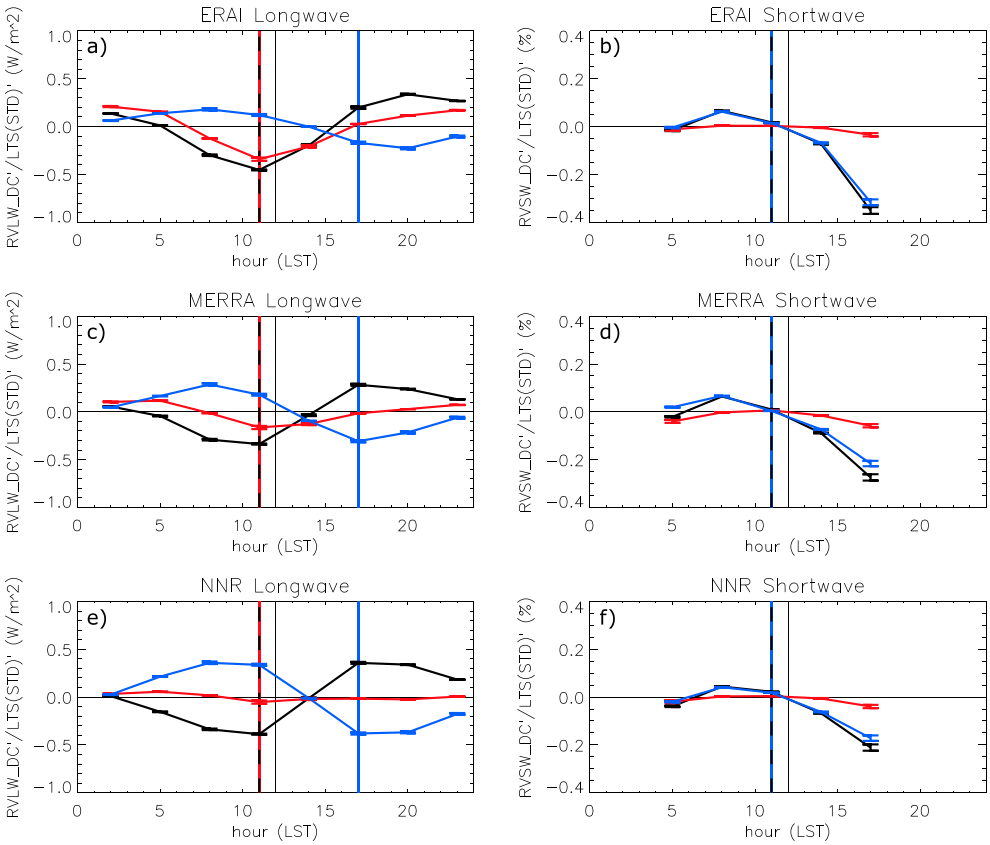


**Figure 5.** As in Figure 3 but with LTS′ as the ASV.

phases of the three curves are the same between FTS′ and CAPE′, the amplitudes are larger. In particular, the amplitude of $LWCF_{DC}$′/FTS′ is about double that of $LWCF_{DC}$′/CAPE′. This results in the amplitude of $OLR_{DC}$′/FTS′ in MERRA being consistent with those of ERA-I and NNR. The effect of $OLR_{DC}$′/FTS′ on $OLR_{DC}$′ is the same (though of opposing sign) as the effect of $OLR_{DC}$′/CAPE′; it primarily shifts the peak time of $OLR_{DC}$′ by a few hours.

As with $RVLW_{DC}$′/FTS′, the $RVSW_{DC}$′/FTS′ curves are generally similar to the $RVSW_{DC}$′/CAPE′ curves, mirrored across the *x* axis, with the exception of NNR. NNR shows a smaller amplitude of $\alpha L_{DC}$′/FTS′ and a slightly different phase—there is no longer a monotonic change in the curve over the day but rather a maximum at 0800 LST and minimum at 1400 LST.

Because FTS is intended to be an alternative measure of vertical instability, the physical meaning of these results is the same as for the CAPE-based results. The fact that the reanalyses show more consistent agreement on the properties of $RV_{DC}$′/FTS′ versus $RV_{DC}$′/CAPE′ supports the idea that FTS is a more reliable measure of vertical instability than CAPE, at least with regard to reanalysis-based results.

### 4.3. LTS

In contrast with $RV_{DC}$′/CAPE′, the results for LTS′ (Figure 5) show more discrepancies between the reanalyses, in both cloud and clear-sky RVs. $LWCF_{DC}$′/LTS′ has notable difference between the reanalyses. All three have a similar phase, with a maximum in late morning and a minimum during evening. NNR shows about twice the amplitude of $LWCF_{DC}$′/LTS′ than MERRA does. In addition, $OLRC_{DC}$′/LTS′ is substantially different between the reanalyses. The phases are similar, but the amplitudes show large differences. NNR shows less than 0.1 W $m^{-2}$ of amplitude, and ERA-I has an amplitude over 5 times that of NNR. MERRA has an amplitude about half that of ERA-I.

Despite these differences, the $OLR_{DC}$′/LTS′ diurnal cycles are similar between the reanalyses, with evening maxima and noon minima. All three reanalyses show a rapid transition from noon to evening and a slow

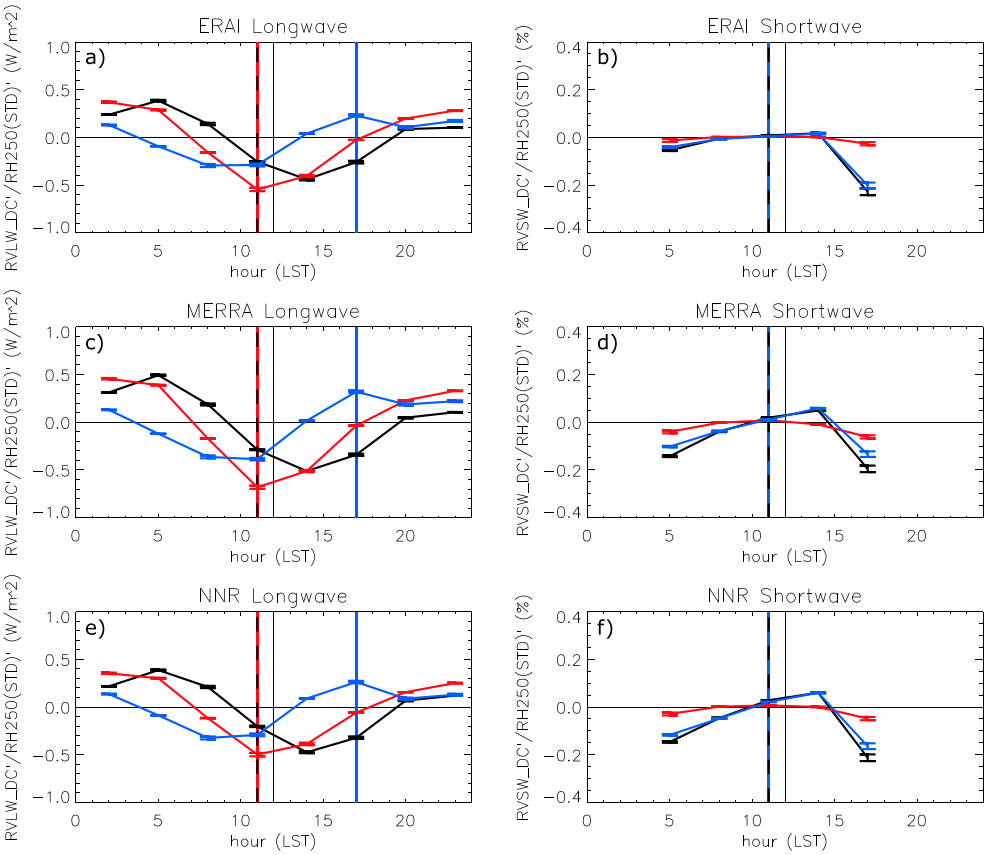


**Figure 6.** As in Figure 3 but with RH250′ as the ASV.

transition from evening to noon. Between ERA-I and NNR, it appears that $LWCF_{DC}$′/LTS′ and $OLRC_{DC}$′/LTS′ offset each other in being the dominant factor in determining $OLR_{DC}$′/LTS′. That is, ERA-I has a larger amplitude of $OLRC_{DC}$′/LTS′ and smaller amplitude of $LWCF_{DC}$′/LTS′, and NNR has vice versa. As a result, $OLR_{DC}$′/LTS′ are similar for both. Thus, the reanalysis choice can significantly skew the attribution of the behavior to clear or cloudy sky.

$RVSW_{DC}$′/LTS′ shows fewer differences between reanalyses than $RVLW_{DC}$′/LTS′. $\alpha L_{DC}$′/LTS′ is the larger contributor to $\alpha_{DC}$′/LTS′, just as with CAPE. Unlike with CAPE, in which $\alpha L_{DC}$′/CAPE′ changes monotonically during the day, $\alpha L_{DC}$′/LTS′ does not change monotonically—it increases from early to midmorning and decreases thereafter. Correspondingly, $\alpha_{DC}$′/LTS′ does the same.

### 4.4. RH250

The amplitudes of $RVLW_{DC}$′/RH250′ are comparable with the amplitudes of the previously shown variables (Figure 6). The curves resemble those of $RVLW_{DC}$′/CAPE′ loosely, though with a couple of important differences. $LWCF_{DC}$′/RH250′ peaks during evening and minimizes during late morning, within 3 h of $LWCF_{DC}$′/CAPE′. The amplitudes of $LWCF_{DC}$′/RH250′ are smaller than $LWCF_{DC}$′/CAPE′ and $LWCF_{DC}$′/FTS′, with the exception of MERRA $LWCF_{DC}$′/CAPE′.

$OLRC_{DC}$′/RH250′ maximizes at night and minimizes around noon, similar to $OLRC_{DC}$′/CAPE′. This is consistent with both relationships being closely tied with convective activity. The larger magnitude of $OLRC_{DC}$′/RH250′ relative to $OLRC_{DC}$′/CAPE′ likely results from the direct radiative effect of UTH, whereas CAPE′ only indirectly influences radiation.

The combined effects of $LWCF_{DC}$′/RH250′ and $OLRC_{DC}$′/RH250′ lead to a maximum of OLR′/RH250′ during midmorning, and a minimum in early afternoon, similar to OLR′/CAPE′. As with CAPE′, because $OLR_{DC}$′/RH250′ does not align with $OLR_{DC}$′, increased (decreased) RH250′ tends to shift the OLR′ diurnal cycle peak earlier (later) in the day. OLRC′/RH250′ is a larger contributing factor to OLR′/RH250′ than OLRC′/CAPE′ is to OLRC′/CAPE′, which

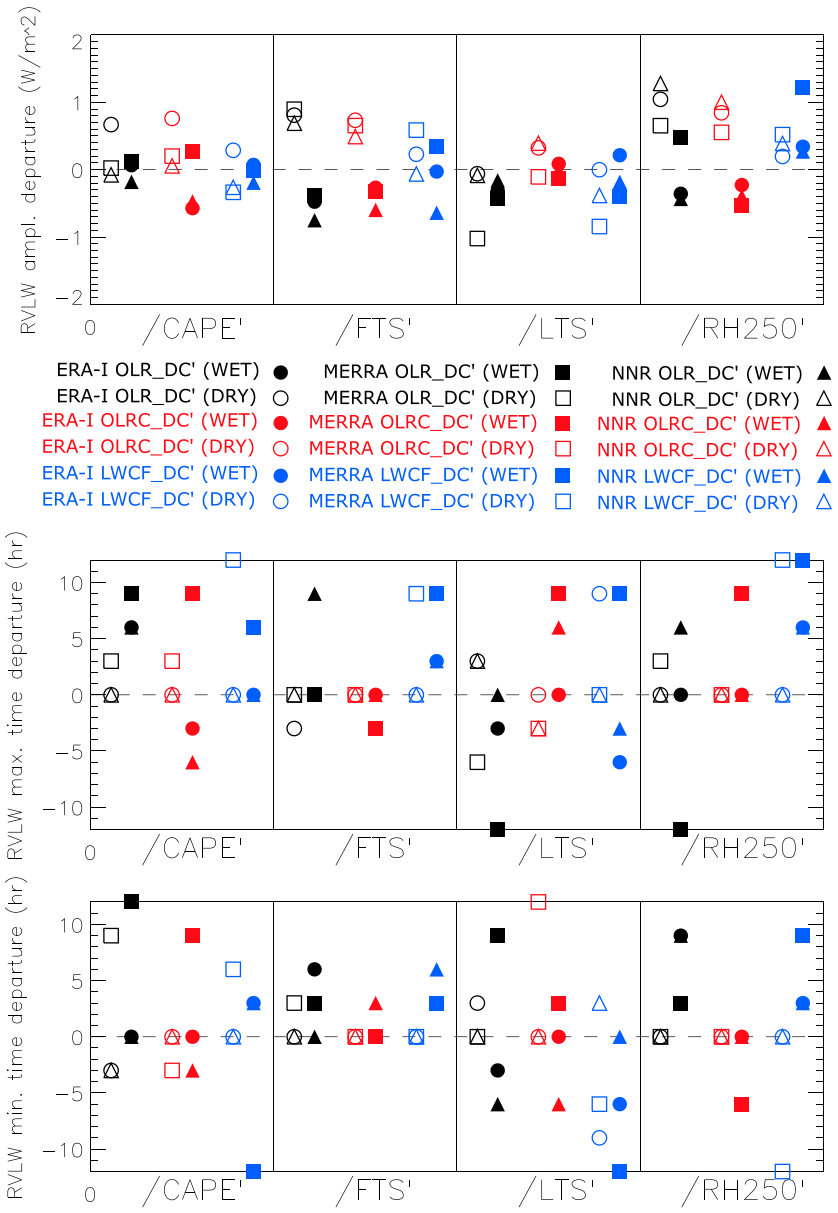


**Figure 7.** The seasonal variability in (top row) amplitude, (middle row) time of diurnal maximum, and (bottom row) diurnal minimum, for $RVLW_{DC}$'/ASV'. $OLR_{DC}$'/ASV' is black, $OLRC_{DC}$'/ASV' is red, and $LWCF_{DC}$'/ASV' is blue. The wet (dry) season is denoted with solid (filled) symbols. Circles represent ERA-I, squares MERRA, and triangles NNR. These results are presented as departures from the quadra-season results—the zero value represents the quadra-season value.

results in a slightly different shape of the curve for $OLR_{DC}$'/RH250'. The minimum is shifted about 3 h earlier in the day with ERA-I and NNR, closer to the time of the $OLRC_{DC}$' minimum.

As with $RVLW_{DC}$'/RH250', $RVSW_{DC}$'/RH250' resembles $RVSW_{DC}$'/CAPE', with more consistency between the reanalyses in the afternoon. $\alpha L_{DC}$'/RH250' and $\alpha_{DC}$'/RH250' increase during the day, with $\alpha C_{DC}$'/RH250' contributing little. The amplitudes of $RVSW_{DC}$'/RH250' are similar to that of $RVSW_{DC}$'/CAPE', though this arises primarily through the decrease in $\alpha L_{DC}$'/RH250' from 1400 to 1700 LST. The curves of $\alpha L_{DC}$'/RH250' are noticeably flatter than those of $\alpha L_{DC}$'/CAPE' from morning to early afternoon, especially for ERA-I. Also, the decrease in $\alpha L_{DC}$'/RH250' from 1400 to 1700 LST is larger than $\alpha L_{DC}$'/CAPE'.

It is reasonable to suspect that the results for $RV_{DC}$'/RH250' are significant only because RH250 and deep convective activity are closely connected; deep convective activity and CAPE (and FTS) are also connected.

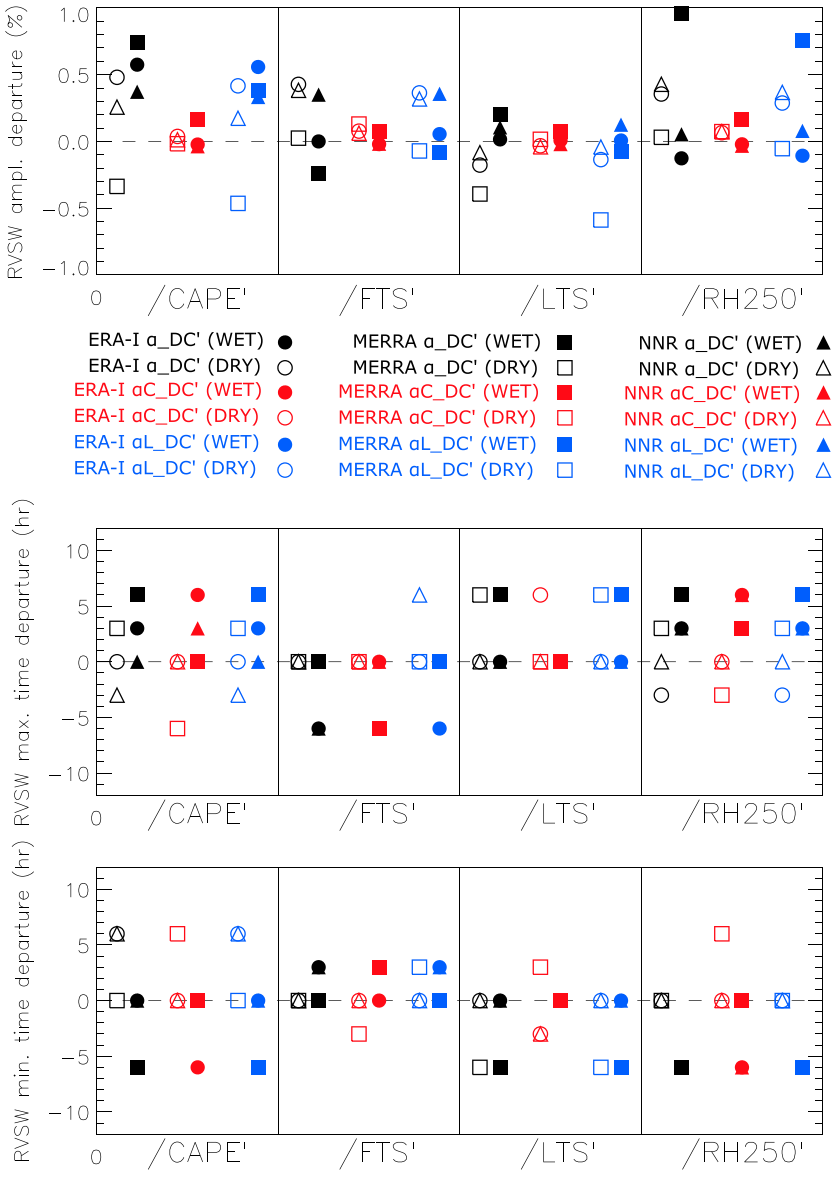


**Figure 8.** As in Figure 8 but for $RVSW_{DC}$'/ASV'. $\alpha_{DC}$'/ASV' is black, $\alpha C_{DC}$'/ASV' is red, and $\alpha L_{DC}$'/ASV' is blue.

Thus, $RV_{DC}$'/RH250' may only be $RV_{DC}$'/CAPE' in "disguise." However, the correlation between RH250' and CAPE' (and FTS') is no more than 0.3 in any of the reanalyses, and scatterplots of the variables suggest no higher-order relationship (not shown). So while RH250' and CAPE' are not entirely independent, the relationship is weak enough that the physical meaning of $RV_{DC}$'/RH250' is distinct from that of $RV_{DC}$'/CAPE'.

## 5. Seasonal Variability in Results

Because the cloud radiative effects (LWCF and $\alpha$L) play a significant role in the total $RV_{DC}$', it is reasonable to suspect that there will be significant differences in the $RV_{DC}$'/ASV' relationships between the wet and dry seasons. The majority of the seasonal results have a similar shape of the diurnal curve as the quadra-season results, and so the seasonal changes in amplitudes, times of maximum, and times of minimum for longwave and shortwave variables are summarized in Figures 7 and 8. The figures show the difference between the quadra-season results and the wet season (filled symbols) and dry season (open symbols) results. For example, Figure 7 shows that NNR, during the wet season, has a $OLR_{DC}$'/CAPE' amplitude that is 0.2 W $m^{-2}$ smaller than

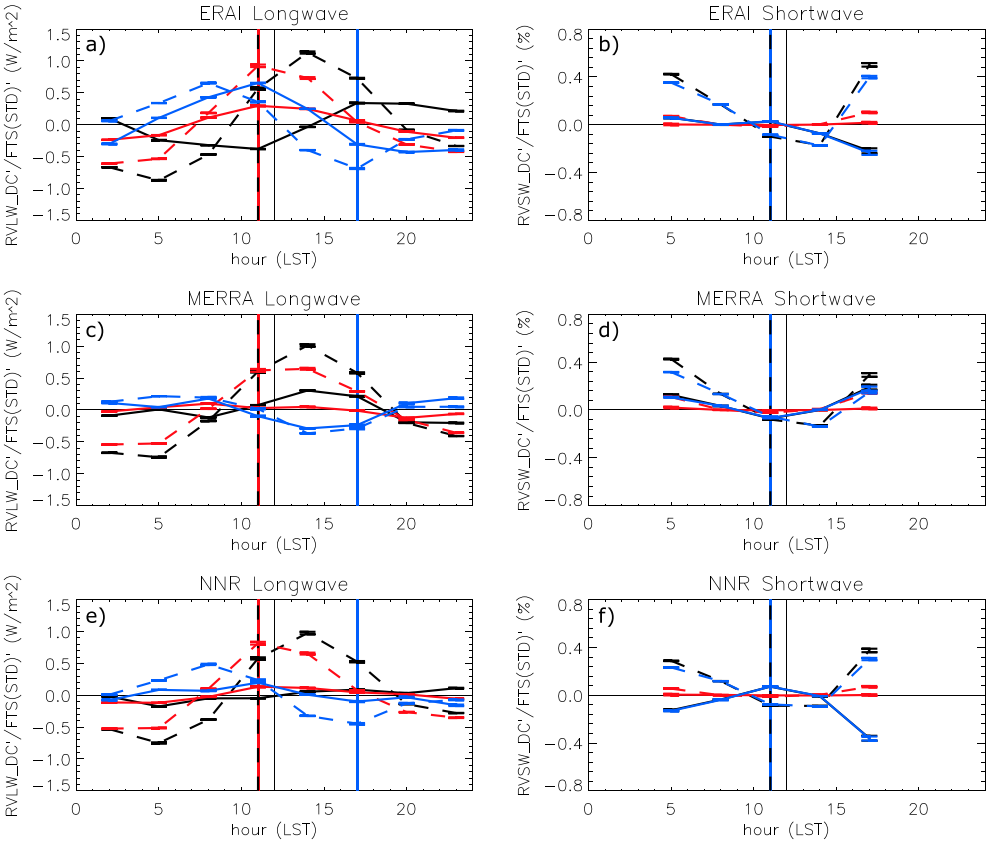


**Figure 9.** As in Figure 4 but with the data subdivided into DJF-only (solid line) and JJA-only (dashed line).

the quadra-season result of ~1.0 W m$^{-2}$, a time of maximum that is 6 h later than the quadra-season results of 0500 LST and a time of minimum that is the same as the quadra-season results of 1700 LST.

### 5.1. Longwave Results

The reanalyses agree within 0.5 W m$^{-2}$ about the seasonal variability in amplitude of $OLR_{DC}$'/LTS', $OLRC_{DC}$'/LTS', $OLR_{DC}$'/RH250', $OLRC_{DC}$'/RH250', and $LWCF_{DC}$'/RH250' (Figure 7). Interestingly, it appears that even in a convectively active region like the Amazon, which possesses a strong seasonal cycle in convective activity, the clear-sky longwave radiative effect is more sensitive to the seasonal cycle than the cloud effect. Because OLRC is strongly associated with surface temperature (TS), we calculated $TS_{DC}$'/ASV' (not shown) and similarly found that the amplitude of the diurnal cycle is much smaller during the wet season than the dry season. So seasonal variability in the amplitude of $TS_{DC}$'/ASV' is causing (or significantly contributing to) variability in the amplitude of $OLRC_{DC}$'/ASV', which is the primary cause of amplitude variability in $OLRC_{DC}$'/ASV'.

There is disagreement between the reanalyses in seasonal amplitude variability larger than 0.5 W m$^{-2}$ for $OLR_{DC}$'/CAPE', $LWCF_{DC}$'/CAPE', $LWCF_{DC}$'/FTS', and $LWCF_{DC}$'/LTS'. This includes disagreements on the sign of the change, most notably MERRA versus NNR for $LWCF_{DC}$'/CAPE' during the dry season. Overall, there appears to be more disagreement between reanalyses in the CAPE-based variables than the FTS-based results, supporting the proposed use of FTS as a more reliable index of convective instability.

The diurnal timing (maximum and minimum) results show that, in general, there is much larger disagreement between the reanalyses during the wet than the dry season. In particular, for both $LWCF_{DC}$'/CAPE' and $LWCF_{DC}$'/FTS', MERRA consistently disagrees with ERA-I and NNR by 6–12 h. This leads to MERRA being the largest outlier in $OLR_{DC}$'/CAPE'.

In general, there is no consistent pattern of seasonal variability in the diurnal timing, as there is in the amplitude. We present the curves for $RV_{DC}$'/FTS' (Figure 9) as an example. Unlike the well-defined diurnal

cycles of $RVLW_{DC}$'/ASV' with obvious maximum and minimum times seen in the quadra-season results, the seasonal results often have multiple maxima/minima and often have no sine curve-like shape. This greatly limits the ability to gather meaningful results and thus draw conclusions on seasonal variability from these data.

### 5.2. Shortwave Results

The $\alpha L_{DC}$'/CAPE' and $\alpha L_{DC}$'/FTS' (and corresponding $\alpha$') results suggest a larger amplitude for some of the reanalyses during both the wet and dry seasons (Figure 8). This unintuitive result can be understood by examining Figure 9. Note that for NNR and (to a lesser extent) ERA-I, the wet and dry season curves have very different values in early morning and late afternoon. $\alpha L_{DC}$'/FTS' for NNR is almost a mirror reflection across the *x* axis between the wet and dry seasons. The quadra-season results fall between the wet and dry season curves, and so the quadra-season amplitude is smaller than the wet and dry amplitudes. MERRA appears to be an outlier for the shortwave results as well as the longwave results (more noticeable in Figure 9 than Figure 8).

All three reanalyses agree that $\alpha L_{DC}$'/RH250' has a larger amplitude during the dry season than wet season (Figure 8). MERRA shows a large seasonal contrast in amplitude for $\alpha L_{DC}$'/LTS', but NNR and ERA-I do not show as large a contrast.

The diurnal timing results again show little consistency between the reanalyses. We might expect that the diurnal timing results would be more difficult to interpret for shortwave than longwave, as the shortwave curves are not sine wave-like curves that shift earlier and later in different seasons. Still, consistency between the diurnal timing indices is expected but is not found. MERRA is most commonly the major outlier, as seen with dry season $\alpha L_{DC}$'/CAPE', wet season $\alpha L_{DC}$'/FTS', and wet season $\alpha L_{DC}$'/RH250'. But this is not always the case, such as with dry season $\alpha L_{DC}$'/LTS'. As with longwave, the shortwave results are too inconsistent to support any conclusions on the seasonal variability of the diurnal timing.

## 6. Discussion

### 6.1. Physical Interpretations of the Results

We can ask the question: do these results make sense in light of currently existing knowledge of what controls the convective diurnal cycle? This is a difficult question to answer comprehensively, as the diurnal cycle can be influenced by a myriad of different processes, both local and nonlocal. However, if we assume that the nonlocal influences over the Amazon are small most of the time, then we can use the conceptual model of the convective diurnal cycle presented by *Chaboureau et al*. [2004] to address this question.

First, the timing of shallow convection initiation is sensitive to both the growth of the atmospheric boundary layer (ABL) and the lifting condensation level (LCL). This period is interesting because the influence of temperature and humidity opposes each other. Increased (decreased) temperature (humidity) increases the height of the LCL. Increased temperature contributes to a deeper boundary layer, but the role of moisture is variable. Increased atmospheric moisture can increase ABL growth through increased buoyancy and eventual cloud formation, but increased soil moisture can slow ABL growth through reducing the Bowen ratio [*Ek and Holtslag*, 2004]. Because of this, it is not immediately obvious that increased temperature and moisture will always result in earlier shallow convection. Conversely, CAPE and FTS always increase from both increased temperature and humidity, by definition. Our results are consistent with increased temperature and humidity shifting shallow convective initiation earlier in the day. This means that increased temperature associated with positive CAPE' (or negative FTS') results in the ABL top reaching the LCL earlier in the day and that increased humidity lowers the LCL without severely stunting ABL growth.

$\alpha_{DC}$'/LTS' is particularly large in the late morning. One potential explanation is that LTS' has a particularly strong effect on shallow boundary layer cumulus (CU) clouds, similar to its effect on marine stratocumulus. In the Amazon, shallow CU are the dominant cloud type during late morning (also demonstrated by *Strong et al*. [2005]), while larger cumuliform clouds and convective anvils develop later in the day, reducing the contribution of shallow CU to the total cloud field. Thus, the effect of LTS' on CU will maximize when the CU cover maximizes.

Second, the transition from shallow to deep convection is sensitive to convective inhibition (CIN) and LFC and involves all five ASVs. Increased convective instability coincides with reduced LFC, so a positive (negative) CAPE′ (FTS′) anomaly should result in the shallow cumulus cloud top reaching the lowered LFC earlier in the afternoon, thus resulting in earlier shallow-to-deep transition. LTS coincides with CIN, so positive LTS′ values usually indicate a positive monthly CIN anomaly. According to *Chaboureau et al*. [2004], the transition from shallow to deep convection does not appear to be triggered by the diurnal minimum of CIN (which occurs earlier in the day) but by turbulence in the ABL growing large enough to overcome CIN. Thus, the higher the CIN anomaly (and by connection, the larger LTS′ anomaly), the later in the day the transition occurs.

As discussed in section 4, the quadra-season results show that positive (negative) CAPE′ (FTS′) has mainly an amplifying effect on $LWCF_{DC}$′. However, note that the minimum (maximum) in $LWCF_{DC}$′/CAPE′ ($LWCF_{DC}$′/FTS′) occurs 3 h before the minimum in $LWCF_{DC}$′. This indicates that a positive anomaly in convective instability shifts the portion of the convective cycle normally occurring at 1100 LST earlier in the day. The time of 1100 LST occurs between the time of shallow cumulus initiation and deep convective initiation, so it might indicate earlier formation of cumulus congestus and young DCCs (preanvil stage). However, these results do not provide evidence that the formation of anvils with large radiative forcing occurs earlier in the day when convective instability is anomalously high. This is consistent with an insensitivity of the precipitation time of maximum to ASVs. The ERA-I quadra-season results show the delay caused by positive LTS′ most strongly, with the minimum in $LWCF_{DC}$′/LTS′ occurring 3 h after the $LWCF_{DC}$′ time of maximum. This corresponds with a shifting of the maximum in $LWCF_{DC}$′ later in the day or a delay in the formation of afternoon DCCs. However, this is not clearly discernable in the MERRA or NNR results. The same is true for the seasonal results.

In addition to this, shallow convection often does not develop immediately into deep convection but often has an intermediary congestus stage. The role of congestus in the diurnal cycle is still being debated [*Waite and Khouider*, 2010; *Hohenegger and Stevens*, 2013; *Ruppert and Johnson*, 2015], but free tropospheric humidity influences the development of congestus into DCCs through modulating dry air entrainment. RH250 is at too high an altitude to directly interact with congestus, but our analysis shows that RH250′ is highly correlated with humidity at lower layers (correlation values of 0.4 and above in our results). Whatever the exact interaction of congestus and the diurnal cycle is, it is reasonable to propose that positive RH250′ should promote the transition from congestus to DCCs, while negative RH250′ suppresses it.

Why should there be a large contrast in the $\alpha L_{DC}$′/CAPE′ and $\alpha L_{DC}$′/FTS′ curves between wet and dry seasons? Recall that in section 4 we suggested that at 1700 LST $\alpha L_{DC}$′/CAPE′ is significantly influenced by the transition from intense DCCs to MCSs and dissipating convective anvils. MCS formation is much more ubiquitous during the wet season than dry season [*Machado et al*., 1998], and the formation of dry season MCSs should be more sensitive to conditional instability. If this is true, then during the wet (dry) season, the increased (decreased) frequency of large, long-lived MCSs across most of Amazonia would result in decreased (increased) $\alpha L_{DC}$′/CAPE′ in the late afternoon. The ERA-I and NNR results both show this (Figures 8a and 8c), but MERRA (Figure 8b) does not.

As with CAPE′ and FTS′, positive RH250′ is associated with an amplification of the convective diurnal cycle, a slightly earlier timing of the late morning convective diurnal cycle, and no change in the time of maximum $LWCF_{DC}$′. In other words, this result implies "lifetime" of the convection is extended. RH250 can be directly connected with deep convection, and thus LWCF, through at least three processes. First, increased deep convection produces more anvil cloud, which evaporates over a few hours and subsequently raises RH250. Second, higher RH250 reduces the evaporation and sublimation rates of the anvil cloud, causing them to persist longer and thus have a larger LWCF. Third, DCCs also influence UTH (of which RH250 represents the uppermost layer) by modulating the rate of dry air entrainment into the convective core. This in turn influences several characteristics of the DCC, including the buoyancy, water content, and microphysics [e.g., *Blyth*, 1993; *Wang et al*., 2007; *Freud et al*., 2011]. These three effects cannot be separated from the results presented, so further investigation, possibly with numerical simulation, will be necessary.

One curious result is that $\alpha L_{DC}$′/RH250′ is smaller in the later afternoon than $\alpha L_{DC}$′/CAPE′. The reason for this is not obvious, because both CAPE′ and RH250′ are closely associated with convection (though not the same,

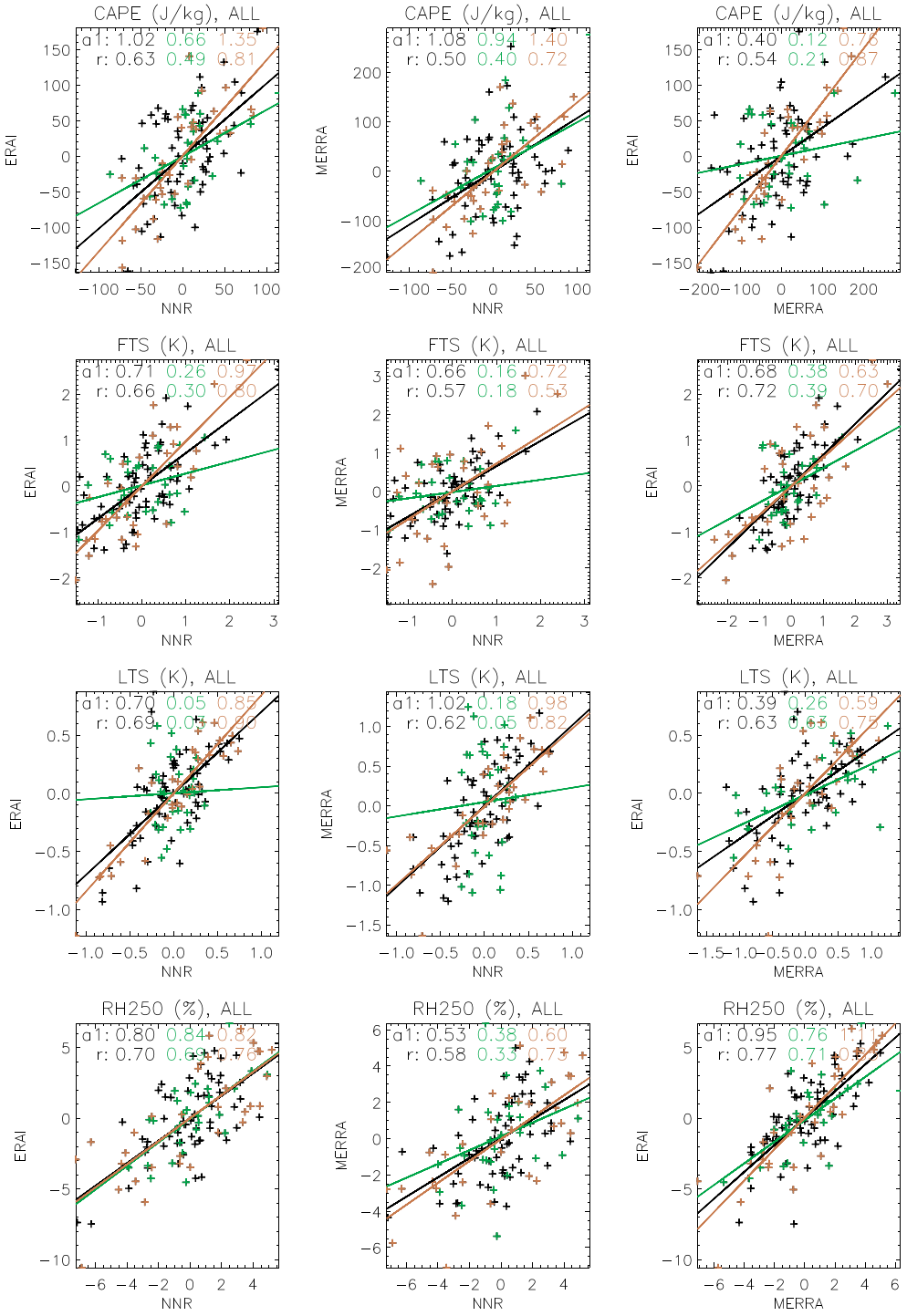


**Figure 10.** Scatterplots and regression lines of (first row) CAPE′, (second row) FTS′, (third row) LTS′, and (fourth row) RH250′, for (left column) NNR versus ERA-I, (middle column) NNR versus MERRA, and (right column) MERRA versus ERA-I. Quadra-season results are shown in black, wet season in green, and dry season in brown. The slopes (*a*1) and correlations (*r*) are shown for each pairing.

as discussed previously). This link is apparent with the $RVLW_{DC}'$, but why should $\alpha L_{DC}'$ be different? One possible explanation for this difference is that RH250 is more directly related to optically thin cirrus than optically thick DCCs and MCSs, as compared with CAPE. So increased afternoon anvil cover associated with positive RH250′ would not increase $LWCF_{DC}'$ as much as increased afternoon DCCs and MCSs associated with positive CAPE′.

### 6.2. Implications for the Results of *Taylor* [2014b]

Recall the hypothesis that $OLR_{DC}'$/CAPE′ tends to shift the OLR′ maximum earlier in the day when CAPE′ is large, and this is thought to be the result of deep convection occurring earlier in the day with increased early afternoon vertical instability. These results generally support this hypothesis. The results show that the time of minimum for $OLRC_{DC}'$/ASV′ (or time of maximum for $OLRC_{DC}'$/FTS′) generally occurs simultaneously of the time of maximum for both $OLRC_{DC}'$ and $OLR_{DC}'$, while the time of minimum for $LWCF_{DC}'$/ASV′ is offset by 3 h. Also, the maximum time of $LWCF_{DC}'$/ASV′ falls within 3–9 h of the OLR′ minimum and the minimum time of $OLRC_{DC}'$/ASV′ within 0–3 h. These results combined can be interpreted to mean that the more important direct cause of the diurnal timing shift in $OLR_{DC}'$ is the cloud effect, not the clear-sky effect. However, the clear-sky effect significantly controls the amplitude of $OLR_{DC}'$. It appears that $OLRC_{DC}'$/ASV′ opposes $LWCF_{DC}'$/ASV′ in altering the amplitude of $OLR_{DC}'$. This distinction is important when understanding the wet season versus dry season results. Because $LWCF_{DC}'$ is smaller during the dry than wet season, variability in ASV′ contributes more to shifting the amplitude of $OLR_{DC}'$ than altering the timing during the dry season (and vice versa).

One of the main questions we have investigated is the seasonal variability in the $RV_{DC}'$/ASV′ relationships. Unfortunately, the results indicate a low reliability of the reanalyses when subsetted into seasons, which reduces sample size. We performed sensitivity tests of the quadra-season results to the number of years included and found substantial variability in the results when the number of years is reduced by more than half (not shown). It seems that a longer and more reliable reanalysis data record, combined with a longer TOA radiative flux record, is necessary to more definitively answer this question. As far as our results go, we can only draw generalized conclusions about the seasonality in the contributions of $LWCF_{DC}'$/ASV′ and $OLRC_{DC}'$/ASV′ to $OLR_{DC}'$/ASV′, as well as the varying influence of shallow and deep convection on $\alpha L_{DC}'$/ASV′.

Figure 2 demonstrates that the reanalyses generally represent the same climatological statistics for the Amazon (with a couple of exceptions in the wet season), so errors in these statistics cannot be the primary explanation for the disagreements in the results. The disagreements must primarily originate from disagreements in the reanalyses on month-to-month variability of the ASVs. Figure 10 shows the scatterplots, regressions, and correlation values of the ASVs between the different reanalyses during the quadra-, wet, and dry seasons. Perhaps the most immediately obvious characteristic of the graphs is that the regressions tend to be weaker during the wet than dry seasons. This is consistent with the reanalyses having increased difficulties diagnosing realistic ASVs during the wet season because of the prominence of convective clouds and precipitation, which are not well simulated in many atmospheric models. The wet season correlation of CAPE′ between ERA-I and NNR (0.49) is greater than that between MERRA and ERA-I (0.21) and slightly greater than that between MERRA and NNR (0.40). This corresponds with MERRA having a particularly poor representation of $RVLW_{DC}'$/CAPE′ during the wet season. FTS′ has a ~0.2 lower correlation between reanalyses than CAPE′ for NNR versus ERA-I and NNR versus MERRA during the wet season, which is curious given that the use of FTS over CAPE generally provides more consistent results. This further illustrates the limitations of the reanalyses in providing robust results.

It may be possible to constrain the data to boost the agreement between the reanalyses by removing the monthly data when the reanalysis ASV anomalies diverge. We investigate this further in Appendix B.

The results show more consistency between reanalyses for the dry than wet seasons, so conclusions regarding the dry season should be more robust (though we cannot rule out all three reanalyses being consistently wrong in the dry season). Because convective activity minimizes in the dry season, it is not surprising that $LWCF_{DC}'$/ASV′ decreases, as LWCF is smaller. But it is interesting that $OLRC_{DC}'$/ASV′ also increases, enough that $OLR_{DC}'$/ASV′ is larger during the dry season than the quadra-season for some variables. This means that the clear-sky effects cannot be ignored in explaining variability in the radiative diurnal cycle, even in convectively active regions like the Amazon. Because, as mentioned previously, OLRC′ is strongly related to TS′, and TS′ is influenced by many factors (many of which are difficult to observe, e.g., surface heat fluxes), fully explaining that OLRC′ may be a difficult task.

## 7. Conclusions

Determining the details of the radiative diurnal cycle, and the processes that contribute to it, is an ongoing field of study. Recently, *Taylor* [2014b] proposed that in convectively active regions, the monthly variability

in the radiative diurnal cycle is linked to variability in the thermodynamical state of the atmosphere through the influence of the convective diurnal cycle. In order to further investigate the hypothesis, as well as the reliability of the analysis method, we have expanded the methodology to examine both the sensitivity of the results to different reanalyses and the sensitivity of the results to the wet/dry seasons.

The work described here yields the following answers to the questions posed in section 1:

*Are the results found by Taylor* [2014b] *robust when replicated using other reanalysis data sets*?

The quadra-season results are generally consistent between different reanalyses, though there are a few small but notable differences in timing and amplitude. MERRA shows about half the amplitude of $LWCF_{DC}$'/CAPE' and $\alpha L_{DC}$'/CAPE' than ERA-I and NNR do, which reduces the amplitude of $OLR_{DC}$'/CAPE' and $\alpha_{DC}$'/CAPE', respectively. ERA-I disagrees with MERRA and NNR on the relative amplitude contributions of $LWCF_{DC}$'/LTS' and $OLRC_{DC}$'/LTS' to $OLR_{DC}$'/LTS', even when agreeing on the amplitude of $OLR_{DC}$'/LTS'. The reanalyses show an 80% disagreement in the amplitude of $\alpha L_{DC}$'/LTS', leading to similar disagreements in $\alpha_{DC}$'/LTS'. The timing for all $RV_{DC}$'/ASV' agrees to within 3 h, except for $\alpha C_{DC}$'/ASV'. However, the latter is very small compared with $\alpha L_{DC}$'/ASV', so the effect on $\alpha_{DC}$' is small.

*Are there other ASVs that influence the monthly variability of the diurnal cycle as strongly as the ones examined by Taylor* [2014b], *including upper tropospheric ASVs*?

FTS was intended to provide an alternative, more reliable ASV to CAPE for representing convective instability. Fittingly, $FTS_{DC}$'/ASV' shows very similar results as $LTS_{DC}$'/ASV' for all reanalyses. In addition, there is no major discrepancy in amplitude of $LWCF_{DC}$'/FTS' between MERRA and the other reanalyses. RH250' appears to have an effect on $RV_{DC}$' of the same order of magnitude as the other ASVs. Because of the correlation below 0.3 between RH250' and CAPE' (and FTS'), this represents an interaction of upper troposphere monthly variability with radiative variability that is at least partially independent of CAPE' variability.

*What is the seasonal dependence of these results*?

Unfortunately, there is too much inconsistency in the results from different analyses to give a clear answer to this question, particularly for the longwave variables. This leads to an additional conclusion that the investigation of the convective diurnal cycle and convection, in general, and the relationship with ASVs is severely limited by the knowledge of atmospheric state. Meteorological reanalysis *may* provide some useful information when gathered over a large enough time domain, but using smaller time domains can lead to false results. In our case, a decade worth of data is not enough to always draw firm conclusions of the seasonal dependence of $RV_{DC}$'/ASV' relationships.Despite this limitation, the most consistent conclusion for longwave results is that the contribution of $OLRC_{DC}$'/ASV' on $OLR_{DC}$'/ASV' is greatly reduced during the wet season and enhanced during the dry season. This means that even if the convective cycle is the dominant factor in controlling $OLR_{DC}$', its indirect clear-sky radiative effect cannot be ignored. The shortwave results are more consistent. They indicate that during the wet season, the deep convective diurnal cycle influences $\alpha_{DC}$' more strongly, while during the dry season the shallow convective cycle has the stronger influence.

## Appendix A: Decadal Trend Occurrences in MERRA

Monthly MERRA data collected for the Amazon show spurious decadal trends over the 2002–2012 data domain (Figure A1). In comparison, ERA-I and NNR do not have comparable trends (not shown).

These trends are not trivial. For example, MERRA produces an increasing trend in CAPE of 403 J $kg^{-1}$ $decade^{-1}$. This is a substantial fraction of the total variability (519 J $kg^{-1}$ before removing the seasonal cycle, 424 J $kg^{-1}$ after) and may have major implications for using MERRA to examine Amazonian deep convection. There are also significant trends in other ASVs, such as surface air temperature and humidity (not shown).

The MERRA trends appear to be linked with trends in the TOA radiative fluxes in MERRA (not to be confused with the CERES TOA fluxes). Figure A2 shows that the trends in OLR' and $\alpha$' arise primarily from trends in LWCF' and $\alpha$L', respectively. Contributing slightly to the OLR' trend is a small trend in OLRC', which corresponds with a trend in TS' of $-1.8$ K $decade^{-1}$ (not shown). There are no significant trends in TOA insolation, surface emissivity, or surface albedo (not shown). Thus, the most likely cause for the spurious RV trends are spurious

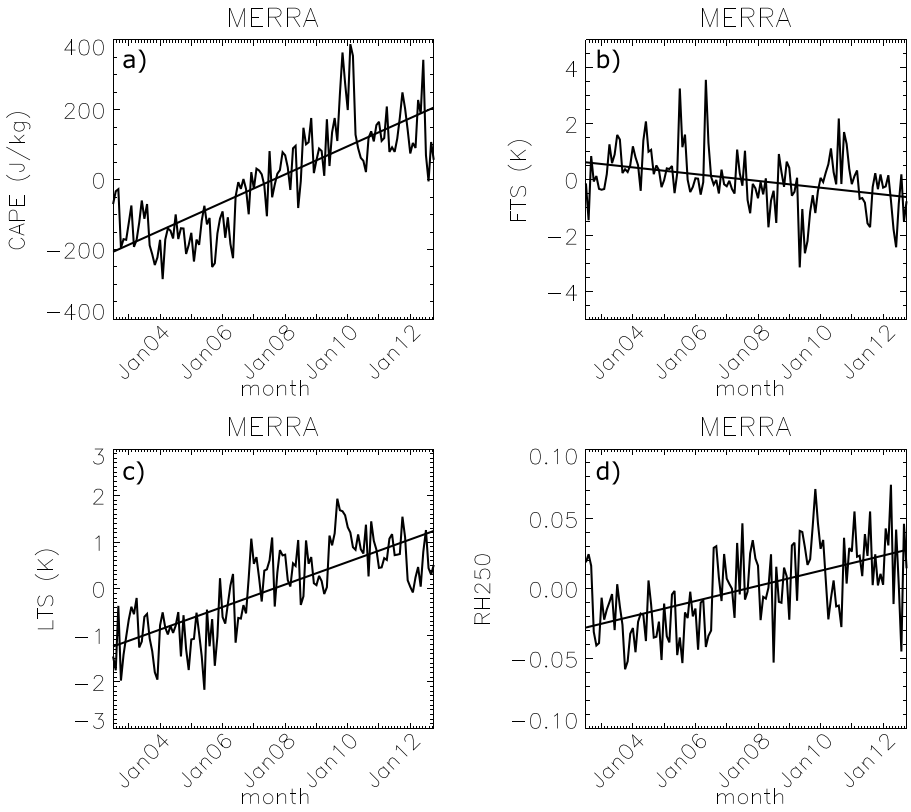


**Figure A1.** Deseasonalized monthly time series and trend lines of (a) CAPE′, (b) FTS′, (c) LTS′, and (d) RH250′ from July 2002 to October 2012.

trends in cloud properties. We have not analyzed MERRA cloud data but suspect that they show decadal trends in Amazonian cloud properties as well.

Unfortunately, with the information presented it is not possible to determine the underlying cause(s) of the RV and ASV trends. It could be errors in cloud simulation influencing the ASVs, or it could be errors in ASVs influencing the clouds, or a combination of the two; or errors in the assimilated data, or data assimilation scheme, or both.

## Appendix B: Improvement of the Seasonal Results Through Forced Agreement of Reanalysis Variables

Figure 10 shows that there are several months in which the reanalyses disagree in both sign and magnitude of ASV anomalies. This is a likely cause of the limited robustness in wet versus dry season results. Would removing the months of disagreement from the data improve the results?

To answer this question, we subset the monthly data based on three sets of criteria. The first criteria set is to use only those months in which all three reanalyses produce the same sign for ASV′. The second set is to use only those months in which all three reanalyses produce ASV′ values within one standard deviation. The third set uses all months that satisfy both the first and second criteria.

For brevity, we show only the wet season results for $RV_{DC}$′/CAPE′ for MERRA, as this was discussed as a particular example of disagreement between the reanalyses. Results derived from other variables and reanalyses are similar. Figure B1 shows that the application of the criteria affects both $OLRC_{DC}$′/CAPE′ and $LWCF_{DC}$′/CAPE′, and the timing of both shifts by 12 h between the unconstrained data (Figure B1a) and the sign-plus-deviation constrained data (Figure B1g). The timing of $LWCF_{DC}$′/CAPE′ shifts to be consistent with ERAA-I and MERRA when the criteria are applied, and correspondingly, the timing of $OLR_{DC}$′/CAPE′ also shifts 12 h, to match the timing shown by ERA-I and NNR. However, also note that the timing of $OLRC_{DC}$′/CAPE′ shifts 12 h from that

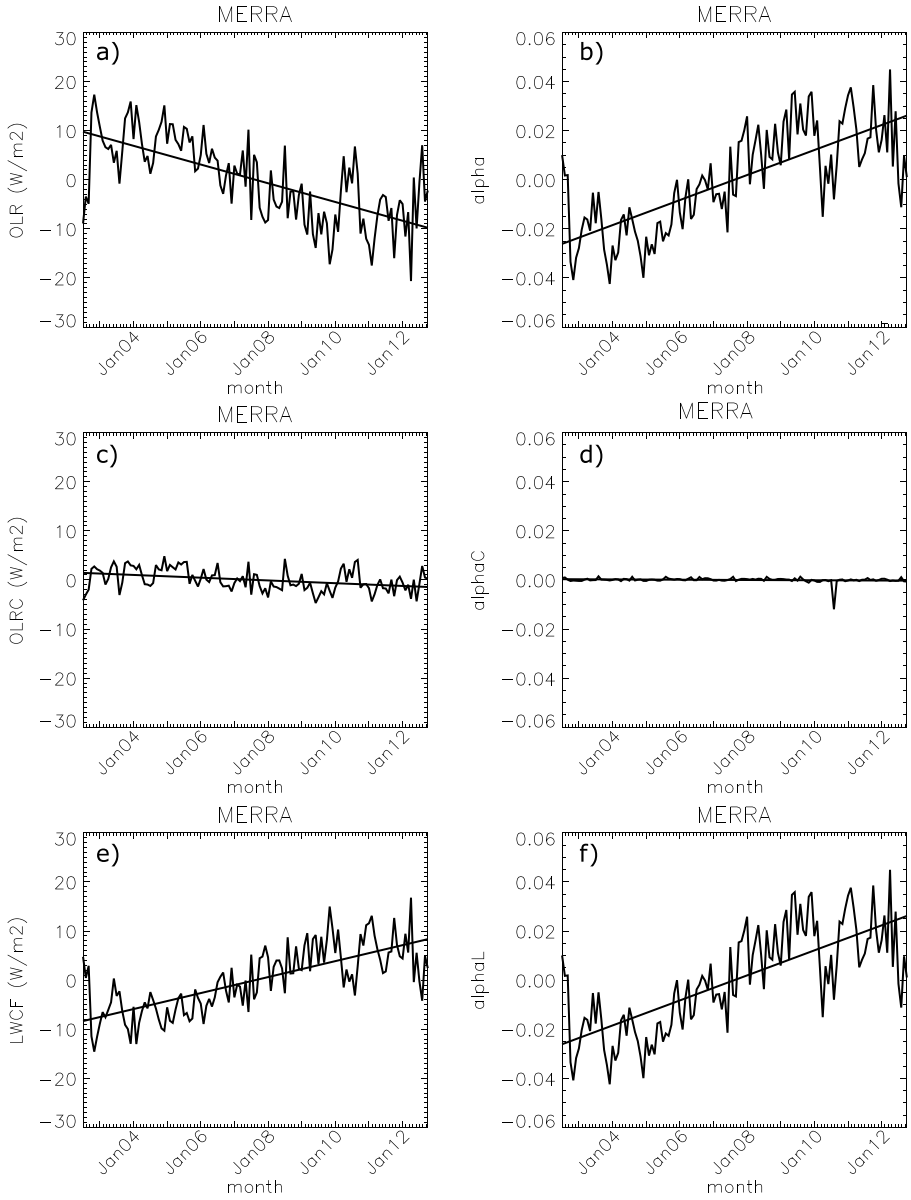


**Figure A2.** Same as Figure A1 but for the RVs.

shown by ERA-I and NNR in Figure B1g, and the amplitude is 50% that of $LWCF_{DC}$'/CAPE'. ERA-I and NNR show the amplitude of $OLRC_{DC}$'/CAPE' to be much less than $LWCF_{DC}$'/CAPE' during the wet season. This is problematic because $OLRC_{DC}$'/CAPE' is the significant control on the diurnal amplitude of $OLR_{DC}$'/CAPE' (see section 6).

Also, $RVSW_{DC}$'/CAPE' is strongly influenced by the use of subsetting. $\alpha L_{DC}$'/CAPE' has a small (relative to NNR and ERA-I) negative slope from late morning to late afternoon using the unconstrained data (Figure B1b), while it has a large positive slope when using the sign-plus-deviation constrained data (Figure B1h). The latter more closely resembles ERA-I and NNR.

Note that because the months included in Figure B1d has been reduced from 30 to 10, the diurnal curves do not resemble sine curves as closely as those produced by the unconstrained data. This complicates the computation of diurnal cycle amplitudes and times of maxima/minima. This may also explain the problematic amplitude and timing of $OLRC_{DC}$'/CAPE'. Nevertheless, these results suggest that improvements in the reliability of reanalysis data will likely result in the improved robustness of results derived from the reanalysis and thus is a worthwhile pursuit.

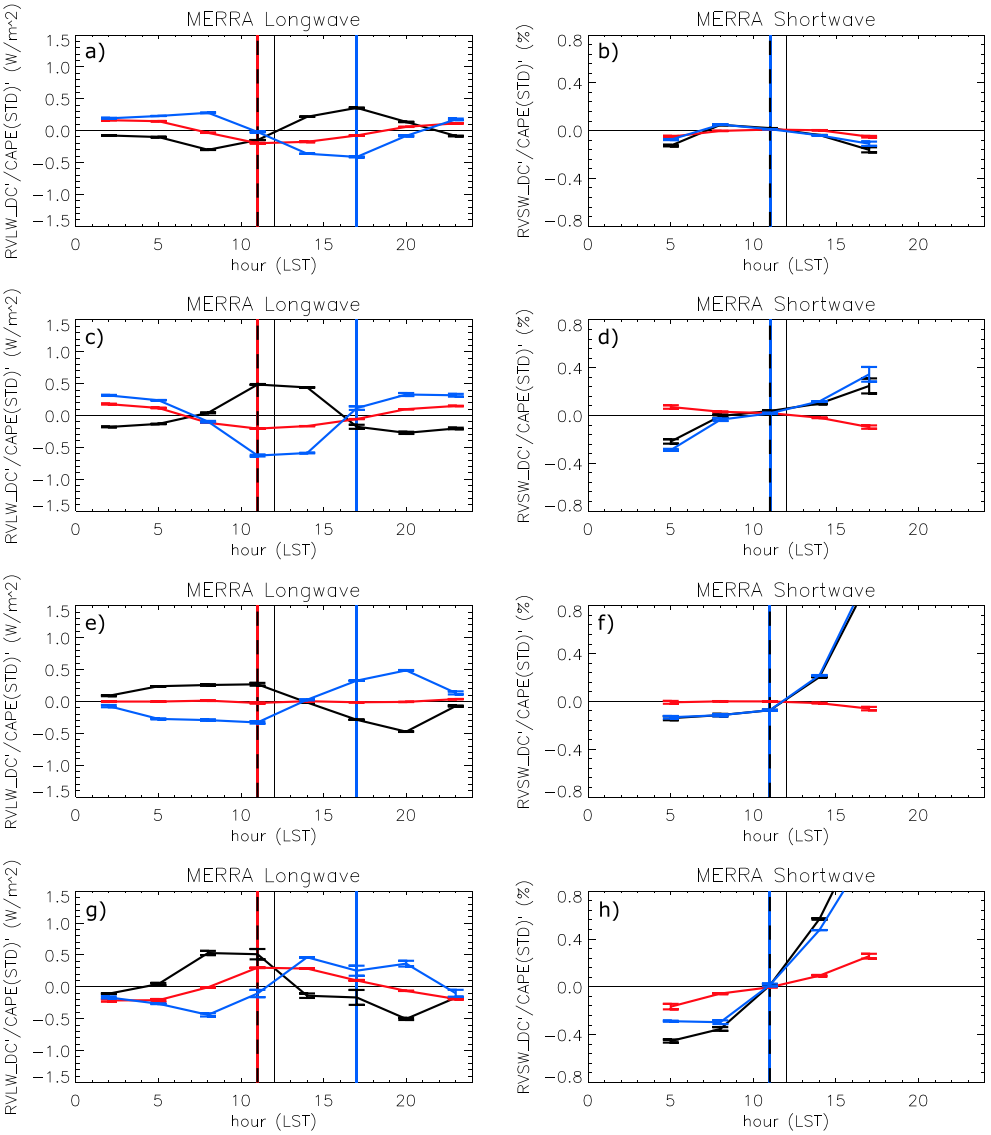


**Figure B1.** Same as Figure 3 but showing the wet season-only results for MERRA applying three sets of subsetting criteria to the data: (a, b) no subsetting, (c, d) only months where the three reanalyses agree on the sign of CAPE′, (e, f) only months where the three reanalyses produce CAPE′ values within one standard deviation of each other, and (g, h) only months which fulfill both previous criteria.

**Acknowledgments**

This work has been supported by NASA grant NNH13ZDA001N-TERAQ, "The Science of Terra and Aqua," and by the NASA Postdoctoral Program. The NNR data were provided by the NOAA/OAR/ESRL PSD, Boulder, Colorado, USA, and are available at http://www.esrl.noaa.gov/psd/. ERA-Interim data used in this study are stored at the ECMWF data server (http://data-portal.ecmwf.int/data/d/interim_mnth/). The MERRA can be obtained from the Goddard Earth Sciences Data and Information Services Center, Greenbelt, Maryland, from their website at http://disc.sci.gsfc.nasa.gov/mdisc. The CERES data used in this study are stored at the Atmospheric Science Data Center at NASA Langley (https://eosweb.larc.nasa.gov).

## References

Balling, R. C., Jr. (1985), Warm season nocturnal precipitation in the Great Plains of the United States, *J. Clim. Appl. Meteorol.*, *24*, 1383–1387, doi:10.1175/1520-0450(1985)024<1383:WSNPIT>2.0.CO;2.

Bergman, J. W., and M. L. Salby (1996), Diurnal variations of cloud cover and their relationship to climatological conditions, *J. Clim.*, *9*, 2802–2820, doi:10.1175/1520-0442(1996)009<2802:DVOCCA>2.0.CO;2.

Bergman, J. W., and M. L. Salby (1997), The role of cloud diurnal variations in the time mean energy budget, *J. Clim.*, *10*, 1114–1124, doi:10.1175/1520-0442(1997)010,1114:TROCDV.2.0.CO;2.

Blyth, A. M. (1993), Entrainment in cumulus clouds, *J. Appl. Meteorol.*, *32*, 626–641, doi:10.1175/1520-0450(1993)032<0626:EICC>2.0.CO;2.

Bony, S., K.-M. Lau, and Y. C. Sud (1997), Sea surface temperature and large-scale circulation influences on tropical greenhouse effect and cloud radiative forcing, *J. Clim.*, *10*, 2055–2077.

Bony, S. A., J.-L. Dufrense, H. Le Treut, J.-J. Morcrette, and C. Senior (2004), On dynamic and thermodynamic components of cloud changes, *Clim. Dyn.*, *22*, 71–86, doi:10.1007/s00382-003-0369-6.

Chaboureau, J.-P., F. Guichard, J.-L. Redelsperger, and J.-P. Lafore (2004), The role of stability and moisture in the diurnal cycle of convection over land, *Q. J. R. Meteorol. Soc.*, *130*, 3105–3117, doi:10.1256/qj.03.132.

Chen, M., R. E. Dickinson, X. Zeng, and A. N. Hahmann (1996), Comparison of precipitation observed over the continental United States to that simulated by a climate model, *J. Clim.*, *9*, 2233–2249, doi:10.1175/1520-0442(1996)009<2233:COPOOT>2.0.CO;2.

Dai (2006), Precipitation characteristics in eighteen coupled climate models, *J. Clim.*, *19*(18), 4605–4630, doi:10.1175/JCLI3884.1.

Dee, D. P., et al. (2011), The ERA-interim reanalysis: Configuration and performance of the data assimilate system, *Q. J. R. Meteorol. Soc.*, *137*, 553–597, doi:10.1002/qj.828.
Del Genio, A. D., Y. Chen, D. Kim, and M.-S. Yao (2012), The MJO transition from shallow to deep convection in CloudSat/CALIPSO data and GISS GCM simulations, *J. Clim.*, *25*, 3755–3770, doi:10.1175/JCLI-D-11-00384.1.
Dirmeyer, P. A., et al. (2012), Simulating the diurnal cycle in global climate models: Resolution versus parameterization, *Clim. Dyn.*, *39*, 399–418, doi:10.1007/s00382-011-1127-9.
Dodson, J. B., D. A. Randall, and K. Suzuki (2013), Comparison of observed and simulated tropical cumuliform clouds by CloudSat and NICAM, *J. Geophys. Res. Atmos.*, *118*, 1852–1867, doi:10.1002/jgrd.50121.
Doelling, D. R., N. G. Loeb, D. F. Keyes, M. L. Nordeen, D. Morstad, C. Nguyen, B. A. Wielicki, D. F. Young, and M. Sun (2013), Geostationary enhanced temporal interpolation for CERES flux products, *J. Atmos. Oceanic Technol.*, *30*, 1072–1090, doi:10.1175/JTECH-D-12-00136.1.
Dolinar, E. K., X. Dong, and B. Xi (2015), Evaluation and intercomparison of clouds, precipitation, and radiation budgets in recent reanalyses using satellite-surface observations, *Clim. Dyn.*, doi:10.1007/s00382-015-2693-z.
Doswell, C. A., III, and E. N. Rasmussen (1994), The effect of neglecting the virtual temperature correction on CAPE calculations, *Weather Forecasting*, *9*, 625–629, doi:10.1175/1520-0434(1994)009<0625:TEONTV>2.0.CO;2.
Ek, M. B., and A. A. M. Holtslag (2004), Influence of soil moisture on boundary layer cloud development, *J. Hydrometeorol.*, *5*, 86–99.
Folkins, I., and R. V. Martin (2005), The vertical structure of tropical convection and its impact on the budgets of water vapor and ozone, *J. Atmos. Sci.*, *62*, 1560–1573, doi:10.1175/JAS3407.1.
Freud, E., D. Rosenfeld, and J. R. Kulkarni (2011), Resolving both entrainment-mixing and number of activated CCN in deep convective clouds, *Atmos. Chem. Phys.*, *11*, 12,887–12,900, doi:10.5194/acp-11-12887-2011.
Fueglistaler, S., A. E. Dessler, T. J. Dunkerton, I. Folkins, Q. Fu, and P. W. Mote (2009), Tropical tropopause layer, *Rev. Geophys.*, *47*, RG1004, doi:10.1029/2008RG000267.
Gray, W. M., and R. W. Jacobson Jr. (1977), Diurnal variation of deep cumulus convection, *Mon. Weather Rev.*, *105*, 1171–1188, doi:10.1175/1520-0493(1977)105<1171:DVODCC>2.0.CO;2.
Harries, J. E., et al. (2005), The Geostationary Earth Radiation Budget Project, *Bull. Am. Meteorol. Soc.*, *86*, 945–960.
Hohenegger, C., and B. Stevens (2013), Preconditioning deep convection with cumulus congestus, *J. Atmos. Sci.*, *70*, 448–464, doi:10.1175/JAS-D-12-089.1.
Itterly, K. F., and P. C. Taylor (2014), Evaluation of the tropical TOA flux diurnal cycle in MERRA and ERA-Interim retrospective analyses, *J. Clim.*, *27*, 4781–4796, doi:10.1175/JCLI-D-13-00737.1.
Janowiak, J. E., P. A. Arkin, and M. Morrissey (1994), An examination of the diurnal cycle in oceanic tropical rainfall using satellite and in situ data, *Mon. Weather Rev.*, *122*, 2296–2311, doi:10.1175/1520-0493(1994)122,2296:AEOTDC.2.0.CO;2.
Jiang, J. H., H. Su, C. Zhai, L. Wu, K. Minschwaner, A. M. Molod, and A. M. Tompkins (2015), An assessment of upper troposphere and lower stratosphere water vapor in MERRA, MERRA2, and ECMWF reanalyses using Aura MLS observations, *J. Geophys. Res. Atmos.*, *120*, 11,468–11,485, doi:10.1002/2015JD023752.
Kalnay, E., et al. (1996), The NCEP/NCAR 40-year reanalysis project, *Bull. Am. Meteorol. Soc.*, *77*, 437–471, doi:10.1175/1520-0477(1996)077<0437:TNYRP>2.0.CO;2.
Kennedy, A. D., X. Dong, B. Xi, S. Xie, Y. Zhang, and J. Chen (2011), A comparison of MERRA and NARR reanalyses with the DOE ARM SGP data, *J. Clim.*, *24*, 4541–4557, doi:10.1175/2011JCLI3978.1.
Loeb, N. G., B. A. Wielicki, D. R. Doelling, G. L. Smith, D. F. Keyes, S. Kato, N. Manalo-Smith, and T. Wong (2009), Toward optimal closure of the Earth's top-of-atmosphere radiation budget, *J. Clim.*, *22*, 748–766.
Machado, L. A. T., W. B. Rossow, R. L. Guedes, and A. W. Walker (1998), Life cycle variations of mesoscale convective systems over the Americas, *Mon. Weather Rev.*, *126*, 1630–1654.
Mapes, B. E., and P. Zuidema (1996), Radiative-dynamical consequences of dry tongues in the tropical troposphere, *J. Atmos. Sci.*, *53*, 620–638, doi:10.1175/1520-0469(1996)053<0620:RDCODT>2.0.CO;2.
Minnis, P., and E. F. Harrison (1984), Diurnal variability of regional cloud and clear-sky radiative parameters derived from GOES data. Part I: Analysis method, *J. Clim. Appl. Meteorol.*, *23*, 993–1011, doi:10.1175/1520-0450(1984)023,0993:DVORCA.2.0.CO;2.
Neale, R., and J. Slingo (2003), The maritime continent and its role in the global climate: A GCM study, *J. Clim.*, *16*, 834–848, doi:10.1175/1520-0442(2003)016,0834:TMCAIR.2.0.CO;2.
Nesbitt, S. W., and E. J. Zipser (2003), The diurnal cycle of rainfall and convective intensity according to three years of TRMM measurements, *J. Clim.*, *16*, 1456–1475, doi:10.1175/1520-0442-16.10.1456.
Raval, A., A. H. Oort, and V. Ramaswamy (1994), Observed dependence of outgoing longwave radiation on sea surface temperature and moisture, *J. Clim.*, *7*, 807–821, doi:10.1175/1520-0442(1994)007<0807:ODOOLR>2.0.CO;2.
Rienecker, M. M., et al. (2011), MERRA: NASA's Modern-Era Retrospective Analysis for Research and Applications, *J. Clim.*, *24*, 3624–3648, doi:10.1175/JCLI-D-11-00015.1.
Rozendaal, M. A., C. B. Leovy, and S. A. Klein (1995), An observational study of diurnal variations of marine stratiform cloud, *J. Clim.*, *8*, 1795–1809, doi:10.1175/1520-0442(1995)008<1795:AOSODV>2.0.CO;2.
Ruppert, J. H., Jr., and R. H. Johnson (2015), Diurnally modulated cumulus moistening in the preonset stage of the Madden–Julian Oscillation during DYNAMO, *J. Atmos. Sci.*, *72*, 1622–1647, doi:10.1175/JAS-D-14-0218.1.
Santanello, J. A., Jr., J. Roundy, and P. A. Dirmeyer (2015), Quantifying the land–atmosphere coupling behavior in modern reanalysis products over the U.S. Southern Great Plains, *J. Clim.*, *28*, 5813–5829, doi:10.1175/JCLI-D-14-00680.1.
Sassi, F., M. Salby, and W. G. Read (2001), Relationship between upper tropospheric humidity and deep convection, *J. Geophys. Res.*, *106*, 17,133–17,146, doi:10.1029/2001JD900121.
Soden, B. J., and R. Fu (1995), A satellite analysis of deep convection, upper-tropospheric humidity, and the greenhouse effect, *J. Clim.*, *8*, 2333–2351, doi:10.1175/1520-0442(1995)008<2333:ASAODC>2.0.CO;2.
Strong, C., J. D. Fuentes, M. Garstang, and A. K. Betts (2005), Daytime cycle of low-level clouds and the tropical convective boundary layer in Southwestern Amazonia, *J. Appl. Meteorol.*, *44*, 1607–1619, doi:10.1175/JAM2266.1.
Su, H., J. H. Jiang, D. G. Vane, and G. L. Stephens (2008), Observed vertical structure of tropical oceanic clouds sorted in large-scale regimes, *Geophys. Res. Lett.*, *35*, L24704, doi:10.1029/2008GL035888.
Sun, Y., S. Solomon, A. Dai, and R. Portmann (2005), How often does it rain?, *J. Clim.*, *19*, 916–934.
Taylor, P. C. (2012), Tropical outgoing longwave radiation and longwave cloud forcing diurnal cycles from CERES, *J. Atmos. Sci.*, *69*, 3652–3669, doi:10.1175/JAS-D-12-088.1.
Taylor, P. C. (2014a), Variability of monthly diurnal cycle composites of TOA radiative fluxes in the tropics, *J. Atmos. Sci.*, *71*, 754–776, doi:10.1175/JAS-D-13-0112.1.

Taylor, P. C. (2014b), Variability of regional TOA flux diurnal cycle composites at the monthly time scale, *J. Atmos. Sci.*, *71*, 3484–3498, doi:10.1175/JAS-D-13-0336.1.

Taylor, P. C., and N. G. Loeb (2013), Impact of Sun-synchronous diurnal sampling on tropical TOA flux interannual variability and trends, *J. Clim.*, *26*, 2184–2191, doi:10.1175/JCLI-D-12-00416.1.

Tian, B., B. J. Soden, and X. Wu (2004), Diurnal cycle of convection, clouds, and water vapor in the tropical upper troposphere: Satellites versus a general circulation model, *J. Geophys. Res.*, *109*, D10101, doi:10.1029/2003JD004117.

Trenberth, K. E., A. Dai, R. M. Rasmussen, and D. B. Parsons (2003), The changing character of precipitation, *Bull. Am. Meteorol. Soc.*, *84*, 1205–1217, doi:10.1175/BAMS-84-9-1205.

Waite, M. L., and B. Khouider (2010), The deepening of tropical convection by congestus preconditioning, *J. Atmos. Sci.*, *67*, 2601–2615, doi:10.1175/2010JAS3357.1.

Wang, Y., L. Zhou, and K. Hamilton (2007), Effect of convective entrainment/detrainment on the simulation of the tropical precipitation diurnal cycle, *Mon. Weather Rev.*, *135*, 567–585.

Yang, G.-Y., and J. Slingo (2001), The diurnal cycle in the tropics, *Mon. Weather Rev.*, *129*, 784–801, doi:10.1175/1520-0493(2001)129,0784:TDCITT.2.0.CO;2.

Yang, S., and E. A. Smith (2006), Mechanisms for diurnal variability of global tropical rainfall observed from TRMM, *J. Clim.*, *19*, 5190–5226.

Zhang, Y., S. A. Klein, C. Liu, B. Tian, R. T. Marchand, J. M. Haynes, R. B. McCoy, Y. Zhang, and T. P. Ackerman (2008), On the diurnal cycle of deep convection, high-level cloud, and upper troposphere water vapor in the Multiscale Modeling Framework, *J. Geophys. Res.*, *113*, D16105, doi:10.1029/2008JD009905.

Zhu, Y., R. E. Newell, and W. G. Read (2000), Factors controlling upper-troposphere water vapor, *J. Clim.*, *13*, 836–848.